US Army Corps of Engineers

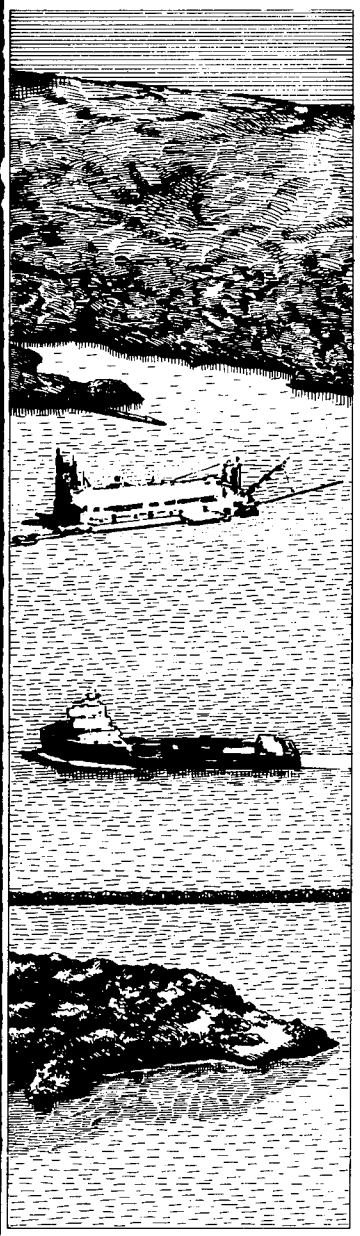

DREDGING RESEARCH PROGRAM

TECHNICAL REPORT DRP-93-1

DEVELOPMENT AND VERIFICATION OF NUMERICAL MODELS FOR PREDICTING THE INITIAL FATE OF DREDGED MATERIAL DISPOSED IN OPEN WATER

Report 2
THEORETICAL DEVELOPMENTS AND VERIFICATION RESULTS

by

Billy H. Johnson, Moira T. Fong

DEPARTMENT OF THE ARMY
Waterways Experiment Station, Corps of Engineers
3909 Halls Ferry Road, Vicksburg, MS 39180-6199

February 1995
Final Report

Prepared for DEPARTMENT OF THE ARMY
U.S. Army Corps of Engineers
Washington, DC 20314-1000

Under Work Unit No. 32465

The Dredging Research Program (DRP) is a seven-year program of the U.S. Army Corps of Engineers. DRP research is managed in these five technical areas:

Area 1 - Analysis of Dredged Material Placed in Open Water
Area 2 - Material Properties Related to Navigation and Dredging
Area 3 - Dredge Plant Equipment and Systems Processes
Area 4 - Vessel Positioning, Survey Controls, and Dredge Monitoring Systems
Area 5 - Management of Dredging Projects

US Army Corps
of Engineers
Waterways Experiment
Station

Dredging Research Program Report Summary

Development and Verification of Numerical Models for Predicting the Initial Fate of Dredged Material Disposed in Open Water; Report 2, Theoretical Developments and Verification Results (TR DRP-93-1)

ISSUE: Numerical models for predicting the initial fate of material disposed in open water are required for the following activities:

- Address environmental concerns related to the disposal of dredged material.
- Provide input for long-term sediment transport models used in disposal site management.

RESEARCH: Dredged material disposal models were developed under the Dredged Material Research Program (DMRP), 1973-1978. Under the Dredging Research Program (DRP), additional developments to the earlier models have resulted in the numerical disposal model called STFATE (Short-Term FATE) for application to split-hull barge and hopper dredge disposal operations. These developments have been guided by both field data and data from large-scale laboratory tests. In addition to guiding model developments, data from the laboratory tests have been used in model validation efforts.

SUMMARY: A numerical model called STFATE (Short-Term FATE) for computing water column concentrations and bottom deposition resulting from a dredged material disposal operation has been developed as a result of extensive modifications to an earlier disposal model. For example, the bottom collapse phase that occurs for most disposals has been redeveloped based upon an energy concept. These developments have been guided by large-scale laboratory tests of disposal operations from a split-hull barge and a multiple bin disposal vessel. Results from the disposal tests have also been employed in model validation efforts. Comparisons of model results with these data are presented in the report.

AVAILABILITY OF REPORT: The report is available through the Interlibrary Loan Service from the U.S. Army Engineer Waterways Experiment Station (WES) Library, telephone number (601) 634-2355. National Technical Information Service (NTIS) numbers may be requested from WES Librarians.

To purchase a copy of this report, call NTIS at (703) 487-4780.

About the Authors: Dr. Billy H. Johnson, WES Hydraulics Laboratory, was Principal Investigator for this work unit and is now Technical Area 1 Manager. Ms. Moira T. Fong is a member of the WES Instrumentation Services Division.

Point of Contact: Dr. Johnson.

For further information on the Dredging Research Program, contact Mr. E. Clark McNair, Jr., Program Manager, at (601) 634-2070.

February 1995

Dredging Research Program

Technical Report DRP-93-1
February 1995

Development and Verification of Numerical Models for Predicting the Initial Fate of Dredged Material Disposed in Open Water

Report 2
Theoretical Developments and Verification Results

by Billy H. Johnson, Moira T. Fong

U.S. Army Corps of Engineers
Waterways Experiment Station
3909 Halls Ferry Road
Vicksburg, MS 39180-6199

Final report

Approved for public release; distribution is unlimited

Prepared for U.S. Army Corps of Engineers
Washington, DC 20314-1000

Under Work Unit No. 32465

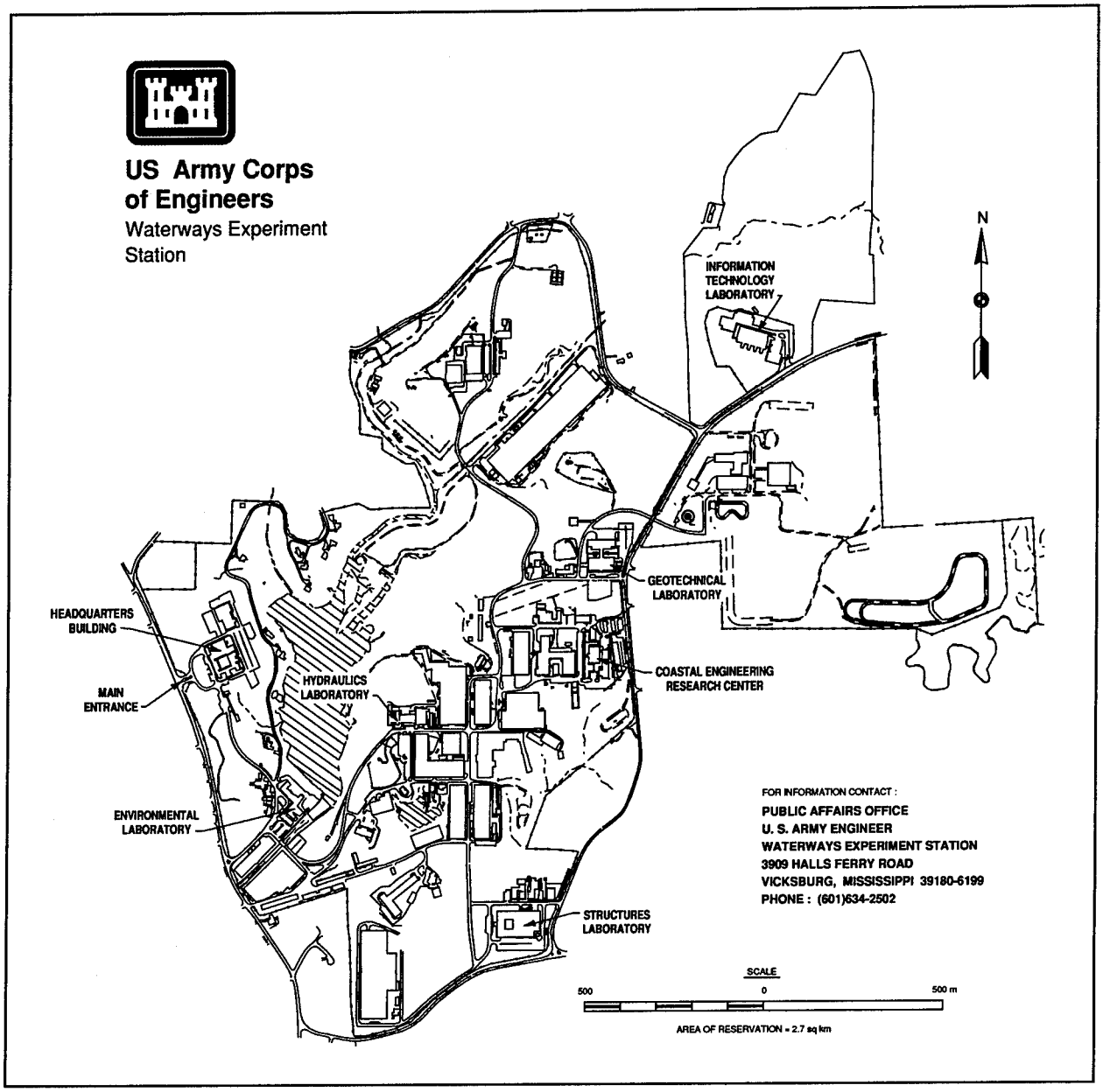

Waterways Experiment Station Cataloging-in-Publication Data

Johnson, Billy H.

Development and verification of numerical models for predicting the initial fate of dredged material disposed in open water. Report 2, Theoretical developments and verification results / by Billy H. Johnson, Moira T. Fong ; prepared for U.S. Army Corps of Engineers.

74 p. : ill. ; 28 cm. — (Technical report ; DRP-93-1 rept. 2)

Includes bibliographic references.

Report 2 of a series.

1. Suspended sediments — Environmental aspects. 2. Dredging spoil — Environmental aspects — Mathematical models. 3. Sedimentation and deposition — Measurement — Mathematical models. I. Fong, Moira T. II. United States. Army. Corps of Engineers. III. U.S. Army Engineer Waterways Experiment Station. IV. Dredging Research Program. V. Title. VI. Title: Theoretical developments and verification results. VII. Series: Technical report (U.S. Army Engineer Waterways Experiment Station) ; DRP-93-1 rept. 2.

TA7 W34 no.DRP-93-1 rept. 2

Contents

Preface

This study was authorized as part of the Dredging Research Program (DRP) of Headquarters, U.S. Army Corps of Engineers (HQUSACE), and was performed under the "Numerical Simulation Techniques for Evaluation of Short-Term Fate and Stabilization of Dredged Material Disposal in Open Waters" Work Unit 32465. This work unit is part of DRP Technical Area 1 (TA1), Analysis of Dredged Material Placed in Open Water. Research was conducted during the period September 1988 to September 1994. Messrs. Robert Campbell and Glenn R. Drummond were DRP Chief and TA1 Technical Monitors from HQUSACE, respectively. Mr. E. Clark McNair, Jr., Coastal Engineering Research Center (CERC), U.S. Army Engineer Waterways Experiment Station (WES), was DRP Program Manager (PM) and Dr. Lyndell Z. Hales, CERC, was Assistant PM. Dr. Nicholas C. Kraus, Senior Scientist, CERC, and Dr. Billy H. Johnson, Hydraulics Laboratory, were Technical Managers for DRP TA1. Dr. Billy H. Johnson, was the Principal Investigator for Work Unit 32465.

At the time of publication of this report, Director of WES was Dr. Robert W. Whalin. Commander was COL Bruce K. Howard, EN.

Additional information can be obtained from Mr. E. Clark McNair, Jr., Program Manager, at (601) 634-2070 or Dr. Billy H. Johnson, Principal Investigator, at (601) 634-3425.

Conversion Factors, Non-SI to SI Units of Measurement

Non-SI units of measurement used in this report can be converted to SI units as follows:

Multiply	By	To Obtain
cubic yards	0.7645549	cubic meters
feet	0.3048	meters
inches	2.54	centimeters
square feet	0.09290304	square meters

Summary

A numerical model called STFATE (Short-Term FATE) for computing water column concentrations and bottom deposition resulting from a dredged material disposal operation has been developed as a result of extensive modifications to an earlier disposal model. For example, the bottom collapse phase that occurs for most disposals has been redeveloped based upon an energy concept. These developments have been guided by large-scale laboratory tests of disposal operations from a split-hull barge and a multiple bin disposal vessel. Results from the disposal tests have also been employed in model validation efforts. Comparisons of model results with these data are presented in the report.

1 Introduction

Background

An integral part of the problem of managing a dredged material disposal site is the ability to determine the physical fate of material immediately after an individual disposal operation and ultimately the long-term movement and/or accumulation of the material deposited initially within the site. The ability to determine the short-term fate of dredged material disposal in open water also is an integral part of assessing the water column environmental impact of disposal operations.

Field evaluations by Bokuniewicz et al. (1978) and laboratory tests by Johnson, et al., (1993) have shown that the placement of dredged material generally follows a three-step process: (a) convective descent during which the material falls under the influence of gravity, (b) dynamic collapse, occurring when the descending cloud or jet either impacts the bottom or arrives at a level of neutral buoyancy, in which case the descent is retarded and horizontal spreading dominates, and (c) passive transport-dispersion, commencing when the material transport and spreading are determined more by ambient currents and turbulence than by the dynamics of the disposal operation. Mathematical models for predicting the short-term fate of material from individual disposal operations that consider these three phases have been developed, e.g., Koh and Chang (1973), Brandsma and Divoky (1976), and Johnson (1990).

A common deficiency of these numerical models is the lack of data for verification and the inadequacy of their representation of the convective descent and collapse phases in real disposal operations. For example, the models developed by Koh and Chang and subsequently modified by Brandsma and Divoky and by Johnson treat the disposal from a split-hull barge as a single hemispherical cloud descending through the water column.

As part of the Dredging Research Program (DRP), physical model disposal tests were conducted at the U.S. Army Engineer Waterways Experiment Station (WES). These tests involved the disposal of various types of material from physical replicates of a split-hull barge and a hopper dredge in a deep

basin. Disposals were made in water depths ranging from 2.0 to 6.0 ft.[1] At a model scale of 1:50, these tests simulated disposal volumes of about 4,000 cu yd from a split-hull barge and 8,000 cu yd from a hopper dredge in water depths of 100 to 300 ft.

Results from eight stationary and seven moving disposals from the model split-hull barge and two stationary and three moving disposals from the hopper vessel are presented by Johnson, et al. (1993). These results consist of information on the short-term dynamics, e.g., average descent and bottom surge speeds, suspended sediment concentrations immediately after disposal, and bottom deposition. Results from these tests have been used to guide the numerical model developments discussed in this report and to provide data for model verification.

Purpose

As previously noted, although model development in this area was initiated in the early 1970's with the work of Koh and Chang (1973) and was continued with developments by Brandsma and Divoky (1976) and Johnson (1990), deficiencies remained. Research in the DRP has been directed at removing many of these model deficiencies, e.g. inadequate representation of disposal from hopper dredges, the inability to represent the nonhomogenity of disposal material, the inability to model disposals at dispersive sites, inadequate representation of the bottom collapse phase, and inability to model disposal over bottom mounds. With the removal of these deficiencies and subsequent model verification employing the laboratory data, accurate predictions of the physical fate of dredged material disposed in open water can be obtained.

Scope

An existing numerical model called DIFID (DIsposal From Instantaneous Dump) has been extensively modified to yield a more versatile, accurate and robust disposal model called STFATE (Short Term FATE). For example, to allow for disposal from hopper dredges and/or a more accurate representation of the disposal material, the concept of multiple convecting clouds that allows for stripping of material during descent has been developed. The resulting model was subsequently verified using laboratory data.

Part II of the report presents theoretical details of the STFATE model. For completeness, all theoretical aspects of the model are presented, although some of the discussion is a reproduction of discussions by Koh and Chang (1973) and Brandsma and Divoky (1976). Verification results from applying the

[1] A table of factors for converting non-SI units of measurement to SI (metric) units is presented on page v.

model to laboratory disposal tests are presented in Part III. Finally, a summary of the model developments and its verification along with conclusions from the study are given.

2 Model Theory

Regardless of the disposal method, the behavior of the disposal material can be separated into three phases: convective descent, during which the disposal cloud or discharge jet falls under the influence of gravity; dynamic collapse, occurring when the descending cloud or jet either impacts the bottom or arrives at a level of neutral buoyancy where descent is retarded and horizontal spreading dominates; and passive transport-dispersion, commencing when the material transport and spreading are determined more by ambient currents and turbulence than by the dynamics of the disposal operation. Figure 1 illustrates these phases.

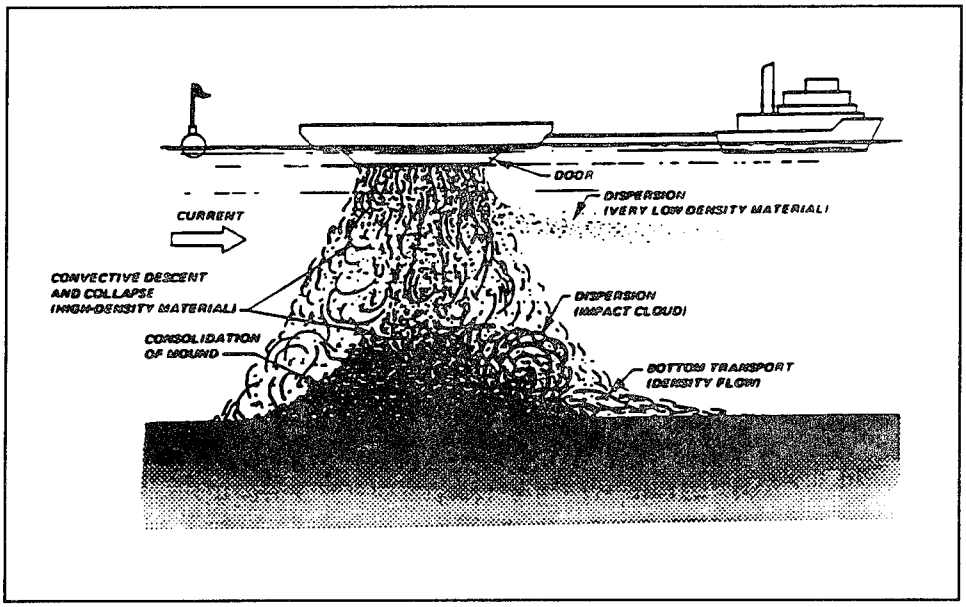

Figure 1. Illustration of placement processes (from Moritz and Randall 1992)

Convective Descent

In STFATE, multiple convecting clouds that maintain a hemispherical

shape during convective descent are assumed to be released. Figure 2 illustrates the basic concept.

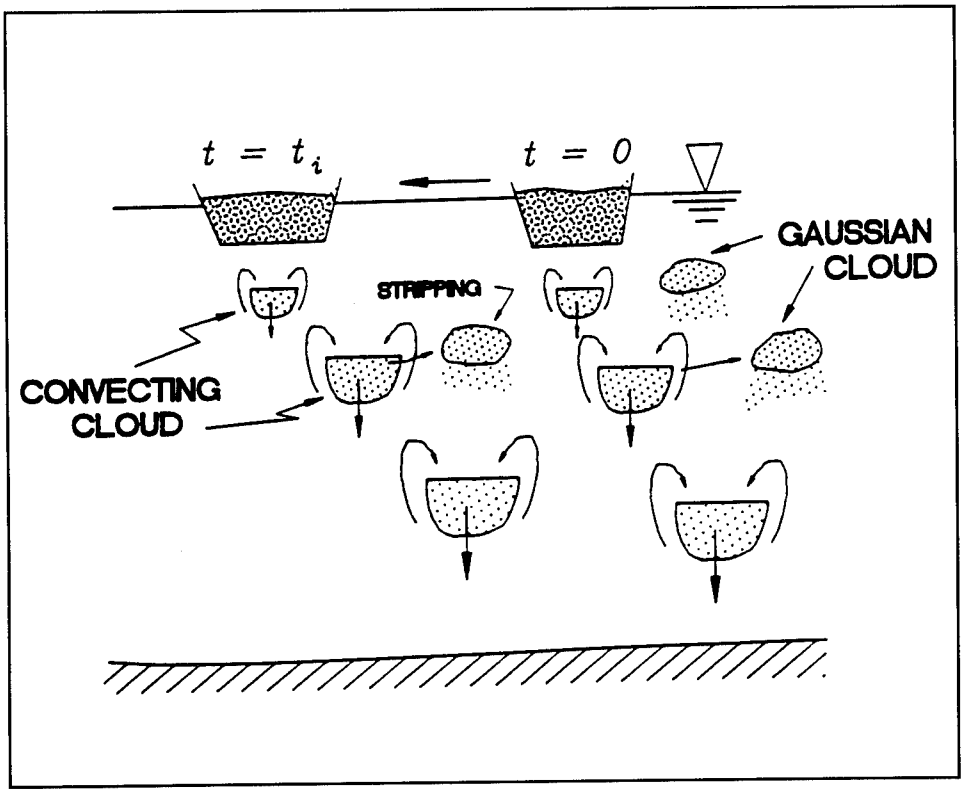

Figure 2. Multiple convecting clouds

By representing the disposal operation as a sequence of convecting clouds, both split hull barge disposal as well as disposal from a hopper dredge can be modeled. For example, the material in each hopper might be contained in one cloud. This concept also allows for a more realistic representation of the disposal material when consolidation has occurred. More dense consolidated material might be represented by one cloud with the less dense more fluid-like fraction overlying the consolidated material represented by a separate cloud. In addition, as illustrated in Figure 2, the use of multiple convecting clouds also allows for a more realistic representation of disposal from a moving vessel where the disposal operation typically requires several seconds to perhaps 1-2 minutes for completion.

As each small convecting cloud descends through the water column, material can be stripped and subsequently settle with its particle settling velocity. Movement of the stripped material as small Gaussian clouds is discussed later.

Other than the concept of multiple convecting clouds and the stripping of material from those clouds, treatment of the convective descent phase for each of the convecting clouds is the same as initially developed by Koh and Chang (1973). For completeness, the governing equations and the following

discussion of these equations are reproduced from Brandsma and Divoky (1976).

The descent analysis is based upon the work of Scorer (1957) and Woodward (1959) in establishing the characteristics of the flow field in and around a buoyant thermal. Their work treated clouds composed entirely of fluid. Since the solids concentration in discharged dredged material is usually low, the cloud is expected to behave as a dense liquid, and the buoyant thermal analysis is appropriate. Figure 3 shows a schematic diagram for the descending hemispherical cloud.

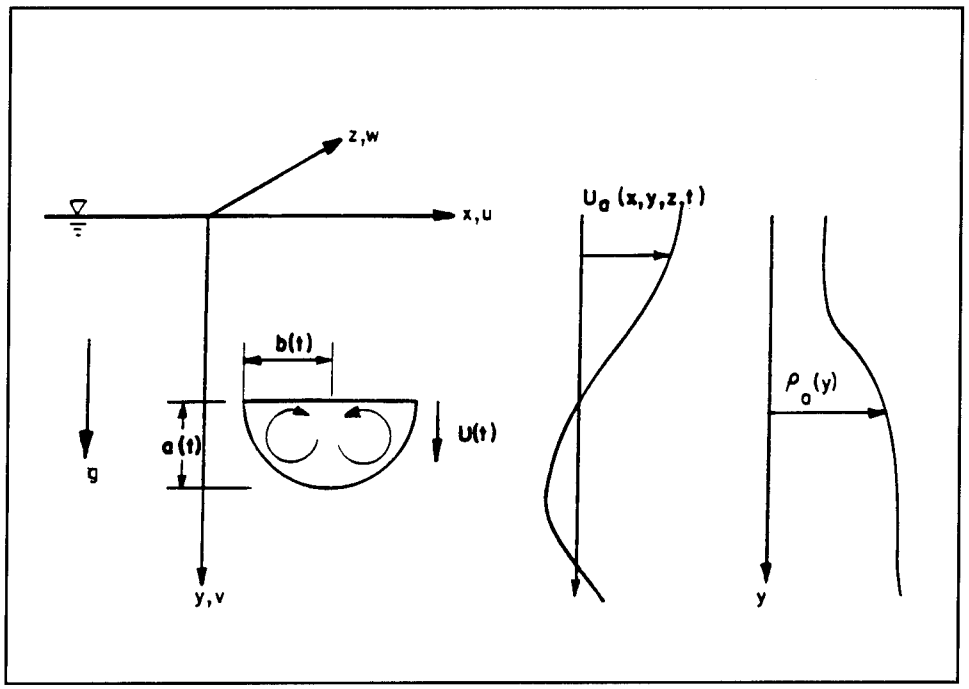

Figure 3. Convective descent (from Brandsma and Divoky 1976)

A mean radius and mean cloud velocity are defined as $a(t)$ and $\vec{U}(t)$ where t is time elapsed since release, $\rho(t)$ is the mean density of the element, and $\rho_a(y)$ is the ambient density. $\bar{U}_a(x,y,z,t)$ is the ambient current, which is assumed to be horizontal and variable in three dimensions and in time. The characteristics of the cloud are assumed to remain similar at all stages of the convective descent. The various solid particles inside are assumed to have densities ρ_i, fall velocities v_{fi}, and concentrations (volume ratio) C_{si}. The equations governing the motion are those for conservation of mass, momentum, buoyancy, solid particles, and vorticity.

The time rate of change of mass in the cloud is the rate of ambient fluid mass entrainment minus the rate of solids mass passing out of the cloud:

$$\frac{d}{dt}(V_c \rho) = E\rho_a - \sum_i S_i \rho_i \quad (1)$$

where the cloud volume is $V_c = \frac{2}{3} \pi a^3$.

The time rate of change of momentum is equal to the buoyancy force minus drag plus the rate of ambient fluid momentum entrainment minus the rate of solids momentum passing out of the cloud:

$$\frac{d\vec{M}}{dt} = F\vec{j} - \vec{D} + E\rho_a \vec{U}_a - \sum_i S_i \rho_i \vec{U} \quad (2)$$

The time rate of change of relative buoyancy is the rate of ambient fluid relative buoyancy entrainment minus the rate of solids relative buoyancy passing out of the cloud:

$$\frac{dB}{dt} = E(\rho_a(0) - \rho_a) - \sum_i (S_i(\rho_a(0) - \rho_i)) \quad (3)$$

The time rate of change of the solid volume of the i^{th} component in the cloud is equal to the rate of the solids volume passing out of the cloud:

$$\frac{dP_i}{dt} = - S_i \quad (4)$$

Several auxiliary equations are used for quantities in the above equations. The rate of entrainment in volume is the product of the surface area of the hemispherical front ($2\pi a^2$), an entrainment coefficient (α), and the magnitude of the velocity difference between the cloud and the ambient fluid:

$$E = 2\pi a^2 \alpha |\vec{U} - \vec{U}_a| \quad (5)$$

The entrainment coefficient will be discussed later in conjunction with the conservation of vorticity equation. The volume rate of solids passing out of the cloud of the i^{th} component is the product of the vertically projected area of the cloud, the magnitude of the fall velocity, the volume fraction of that component in the cloud, and a settling coefficient:

$$S_i = \pi a^2 \, |v_{fi}| \, C_{si}(1-\beta_i) \tag{6}$$

Several additional equations are necessary for the following:

Momentum

$$\vec{M} = C_m \rho \, \frac{2}{3} \pi a^3 \, \vec{U} \tag{7}$$

Buoyancy force

$$F = \frac{2}{3} \pi a^3 g(\rho - \rho_a) \tag{8}$$

Drag force in x-direction

$$D_x = 0.5 \, \rho_a C_D(0.5\pi a^2) \, |\vec{U} - \vec{U}_a| \, (u - u_a) \tag{9}$$

Drag force in y-direction

$$D_y = 0.5 \, \rho_a C_D \pi a^2 \, |\vec{U} - \vec{U}_a| \, v \tag{10}$$

Drag force in z-direction

$$D_z = 0.5 \, \rho_a C_D(0.5\pi a^2) \, |\vec{U} - \vec{U_a}| \, (w - w_a) \tag{11}$$

Buoyancy

$$B = \frac{2}{3} \pi a^3 (\rho_a(0) - \rho) \tag{12}$$

Solid volume of the i^{th} component in the cloud

$$P_i = \frac{2}{3} \pi a^3 C_{si} \tag{13}$$

In the above equations, α is an entrainment coefficient; β_i is a settling coefficient; $\vec{j}$ is the unit vector in the vertical direction; C_D is a drag coefficient; C_m is an apparent mass coefficient; and $\rho_a(o)$ is the density at the free surface. The drag coefficient C_D is a function of Reynolds number and therefore depends on a and $|\vec{U} - \vec{U_a}|$. The value of C_D is suggested to be 0.5. The apparent mass coefficient, C_m, is suggested to be between 1.0 and the value for a sphere, i.e., 1.5.

The last governing equation is that for vorticity. The total vorticity is the cloud's identity-preserving mechanism, and it is also important in determining the amount of entrainment. When a cloud of material is ejected into the ambient fluid, some initial vorticity is generated when passing through the entrance boundary. Total vorticity is generated only by shear forces at the fluid boundaries. Once a cloud is in the ambient fluid, there are two possibilities if the bottom is not encountered. In a uniform density ambient fluid, total vorticity is conserved, although cloud growth acts to diffuse the vortex strength. In a stratified fluid, the density gradient acts to decay the total vorticity according to:

$$\frac{dK}{dt} = - A \epsilon \tag{14}$$

where K is vorticity; A is a dissipation parameter; and ϵ is the density gradient as defined below:

$$A = \frac{Ca^2 g}{\rho_a(0)} \tag{15}$$

$$\varepsilon = \frac{d\rho_a}{dy} \tag{16}$$

C is a vorticity dissipation coefficient which is equal to 3 according to Turner (1960). Vorticity is of concern only because it influences entrainment.

The entrainment coefficient α is dependent upon the properties of the cloud, the properties of the ambient fluid, and the turbulence structure inside and outside the convecting cloud. In formulating an expression for an entrainment coefficient, it is necessary to account for the structure of the cloud as it changes from a vortex ring to a turbulent thermal. Scorer (1957) and Richards (1961) experimentally determined the entrainment coefficient for turbulent thermals, α_o, to be approximately 0.25. In studying the motion of a vortex ring, Turner (1960) found an entrainment coefficient:

$$\alpha = \frac{B}{2\pi\, g\, C_1 K^2} \tag{17}$$

by assuming similarity where C_1 was found to be 0.16. B is the buoyancy and K is the total vorticity. As the cloud descends and its vorticity approaches zero, Turner's assumption of similarity cannot hold. Since α is expected to approach α_0 found in turbulent thermals, Koh and Chang (1973) thought it reasonable to postulate that the dependence of α on B and K might be of the form:

$$\alpha = \alpha_0 \sqrt{\tanh\left(\frac{B}{2\pi g C_1 K^2 \alpha_0}\right)^2} \tag{18}$$

Their only justification for Equation 18 was that it tends to the correct limits: to Turner's relation when K is large and to α_0 when K is small.

Laboratory studies by Bowers and Goldenblatt (1978) resulted in the following empirically derived expression for the entrainment coefficient.

$$\alpha = 0.285 + 0.00493\ (MLL - 2.9) \tag{19}$$

where MLL = Multiple of Liquid Limit. This expression results in a maximum value of about 0.30. However, Kraus (1991) determined entrainment

coefficients of about 0.60 from field data collected at Mobile Bay. As noted later, the larger value is required to achieve volume increases of 50 to 70 times the disposal volume as observed by Bokuniewicz, et al. (1978) and Johnson, et al. (1993).

Koh and Chang used dimensional analysis to show that the dimensionless mass rate of settling is a function of the ratio of the descending velocity of the cloud, v; the fall velocity of the solid particles, v_{fi}; the concentration of each group of particles, C_{si}; and total concentration, C:

$$\frac{q}{v_{fi}\rho_i a^2} = \pi C_{si}(1 - \beta_i) \tag{20}$$

where β_i is defined to be a settling coefficient which depends upon v/v_{fi}, C_{si}, and C. β_i is expected to be between 0 and 1, representing the two cases of settling freely or no settling.

Therefore,

$$\beta_i = \begin{cases} 0 & if \quad \left|\frac{v}{v_{fi}}\right| < 1 \\ 1 & if \quad \left|\frac{v}{v_{fi}}\right| \geq 1 \end{cases} \tag{21}$$

Given a set of initial conditions, e.g., the total volume of disposal material, sediment concentrations, etc., Equations 1-4 along with Equation 14 can be solved using numerical techniques. In STFATE, the forward Euler scheme is used. Earlier work by Koh and Chang employed a fourth order Runga-Kutta scheme. However, testing over a range of disposal volumes and water depths revealed little difference in the computed results and the first order Euler scheme appeared to be more robust. Given the idealized representation of the disposal operation and the uncertainty of initial conditions, the need for higher-order numerical schemes is questionable.

Bokuniewicz, et al. (1978) found that the insertion speed was an important variable. Therefore, special attention has been directed at computing the cloud insertion speed in STFATE.

Consider Figure 4, with A_o being the inside area of the disposal vessel, A_1 being the area of the opening, h the height of the disposal material, d the vessel draft, p_o the atmospheric pressure, and V_o and V_1 velocities at the surface and at the opening respectively.

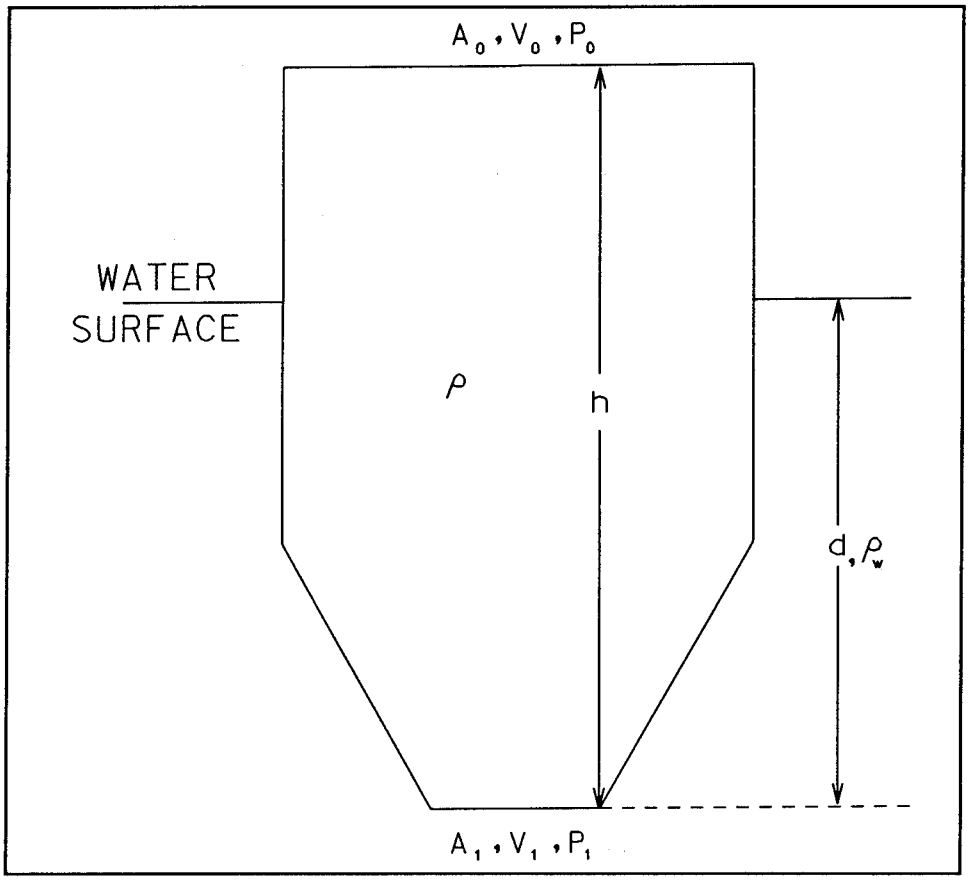

Figure 4. Computation of insertion speed

The energy equation can be written as

$$h + \frac{P_o}{\gamma_s} + \frac{V_o^2}{2g} = \frac{P_1}{\gamma_s} + \frac{V_1^2}{2g} + \varepsilon \tag{22}$$

where, at the moment the doors are opened, the pressure at the opening, P_1, is

$$P_1 = P_o + \rho_w g d \tag{23}$$

Therefore,

$$h + \frac{V_o^2}{2g} = \frac{\rho_w}{\rho_s} d + \frac{V_1^2}{2g} + \varepsilon \tag{24}$$

where ε is the energy lost due to friction as the material passes through the opening.

From continuity,

$$A_o V_o = A_1 V_1 \tag{25}$$

Thus Equation 24 can be solved for V_1 to yield

$$V_1 = \left\{ \frac{2g \left(h - \frac{\rho_w}{\rho_s} d - \varepsilon \right)^{1/2}}{\left[1 - \left(\frac{A_1}{A_o} \right)^2 \right]} \right\} \tag{26}$$

Before the doors are opened, the mass of the boat and the disposal material must equal the mass of the water displaced, i.e.,

$$d \rho_w \bar{A} = h \rho_s A_o + \textit{mass of boat} \tag{27}$$

or

$$h = \frac{\rho_w d \bar{A}}{\rho_s A_o} - \textit{unloaded draft} \tag{28}$$

where $\bar{A}$ = area of the vessel at the water line. Therefore, as convecting clouds are released, changes in h and d are related by

$$\Delta h = \frac{\rho_w \bar{A}}{\rho_s A_o} \Delta d \tag{29}$$

The energy loss, ε, is estimated by

$$\varepsilon = \frac{1}{2} V_1^2 \rho f \tag{30}$$

where f is the friction factor. For fully turbulent flow, f is approximately 0.02. Substituting Equation 30 into Equation 26 and solving for V_1 yields the expression employed in STFATE for the insertion velocity.

$$V_1 = \left\{ \frac{\rho_{AV} g h - \rho_w g d}{1/2 \rho_{AV} \left[1.0 + f - \left(\frac{A_1}{A_o} \right)^2 \right]} \right\} \tag{31}$$

where the average density of the disposal material remaining in the vessel is computed from

$$\rho_{AV} = \frac{\rho_B Vol_T - \sum_{i=1}^{NLAY} \rho_i Vol_i}{Vol_T - \sum_{i=1}^{NLAY} V_i} \tag{32}$$

where ρ_B is the average or bulk density of the entire load, Vol_T is the total volume being disposed, and ρ_i and Vol_i are the average density and volume of the individual layers in the disposal vessel. Each layer ultimately becomes a convecting cloud.

Dynamic Collapse in Water Column

As the disposal cloud goes through the convective descent phase, it gains mass and momentum by entrainment. The horizontal velocity of the cloud

tends to approach that of the ambient fluid. Coincidently, the waste material concentration is greatly reduced and the vorticity becomes insignificant because of dissipation by ambient stratification and turbulence. If the cloud reaches the depth of neutral buoyancy, its momentum will tend to make it overshoot beyond the neutrally buoyant point while the buoyancy force will tend to bring it back to the neutrally buoyant position. The combined action of these forces will make the cloud undergo a decaying vertical oscillation. As the vertical motion of the cloud is being suppressed, the cloud tends to collapse vertically and spread out horizontally, seeking hydrostatic equilibrium within the stratified ambient fluid. As the cloud collapses, its cross section becomes elongated in the horizontal, and another dimension is needed to describe the cloud shape. If the cross section of the cloud is assumed to be elliptical, its shape may be characterized by its semi-major and semi-minor axes, b and a, respectively (Figure 5).

It is assumed that the cloud always retains the shape of an oblate spheroid. If coordinate axes are chosen to originate from the cloud centroid, the cross-sectional outline of the cloud may be represented by

$$\frac{y'^2}{a^2} + \frac{r'^2}{b^2} = 1 \tag{33}$$

where a and b vary with time. The cloud is assumed to remain symmetrical, which in practice will only be true if there is no relative velocity between the cloud and the ambient fluid and therefore no velocity shear. Following convective descent, the velocity difference between the cloud and the ambient fluid is expected to be small, and its influence on shape can be neglected.

With the exception of vorticity, the conservation equations used for convective descent still hold. Any differences are due to the additional dimension used to describe the cloud. The conservation equations are:

Conservation of mass

$$\frac{d}{dt}(V_c \rho) = E \rho_a - \sum_i S_i \rho_i \tag{34}$$

where the cloud Volume $V_c = \frac{4}{3} \pi ab^2$.

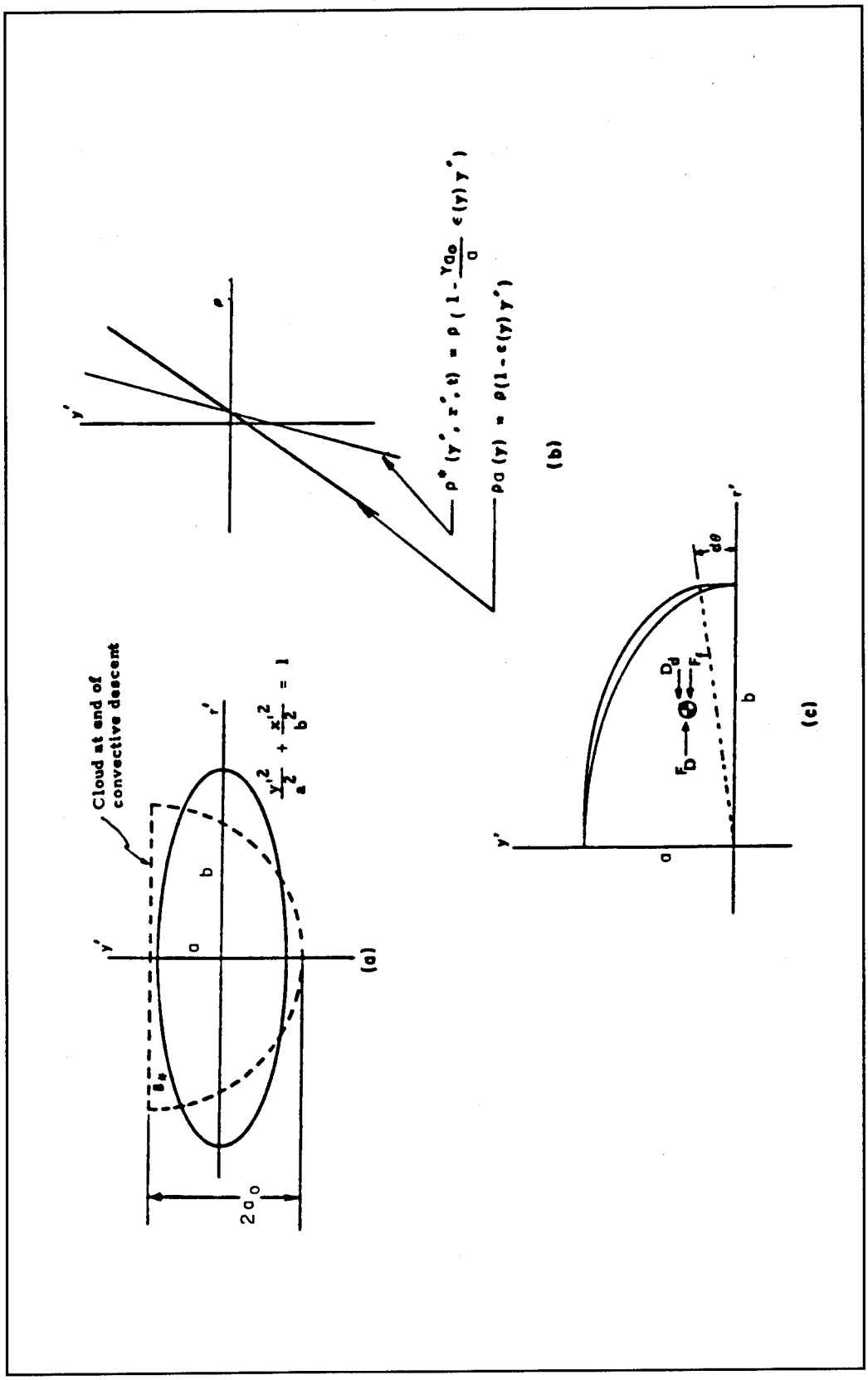

Figure 5. Aspects of cloud collapse (from Brandsma and Divoky (1976))

Conservation of momentum

$$\frac{d\vec{M}}{dt} = \vec{Fj} - \vec{D} + E\rho_a \vec{U_a} - \sum_i S_i \rho_i \vec{U} \tag{35}$$

Conservation of buoyancy

$$\frac{dB}{dt} = E(\rho_a(0) - \rho_a) - \sum_i S_i(\rho_a(0) - \rho_i) \tag{36}$$

Conservation of solid particles

$$\frac{dP_i}{dt} = - S_i \tag{37}$$

The major auxiliary equations are those for entrainment of ambient fluid, for the settling of solid particles, and for the collapse of the cloud.

The two contributions to entrainment come from movement of the entire cloud through the ambient fluid and from the additional velocity shear at the cloud boundary due to the cloud collapse. Each contribution is the product of the surface area of the cloud, an entrainment coefficient, and a velocity. The expression for the rate of entrainment of ambient fluid is:

$$E = \left\{ 2\pi\, b^2 + \pi\, \frac{a^2 b}{R} \ln\left(\frac{b+R}{b-R}\right) \right\} \left(\alpha\, |\vec{U} - \vec{U_a}| + \alpha_c \frac{db}{dt} \right) \tag{38}$$

where $R = \sqrt{b^2 - a^2}$; α is the entrainment coefficient for cloud motion; and $|\vec{U} - \vec{U}_a|$ is the magnitude of the velocity difference between the cloud and the ambient fluid. α_c is introduced into the formulation to account for the entrainment due to collapse, and *db/dt* is the velocity of the tip of the collapsing cloud. It is assumed that entrainment due to the cloud motion should die out as the cloud settles into the neutral buoyancy position. This may be done by letting the entrainment coefficient be:

$$\alpha = \left[\frac{a}{b}\right]^2 \alpha_0 \tag{39}$$

where α_0 is the entrainment coefficient for a turbulent thermal. This relation is employed merely as an effective way to turn off entrainment due to cloud motion.

As in the section on convective descent, the volume rate of solids settling out of the cloud is

$$S_i = \pi b^2 \, |v_{fi}| \, C_{si} \, (1 - \beta_i) \tag{40}$$

where β_i is the settling coefficient defined by Equation 21.

The mechanism that drives the collapse of the cloud within the water column is the density difference between the inside and outside of the cloud. It is assumed that, because of the turbulent mixing, the density gradient inside the cloud is less than that outside. Assume that the cloud is resting at the level of neutral buoyancy and that the ambient density at this level is ρ_0. Assume further that the density gradients inside and outside of the cloud are of constant magnitude. Let ϵ be the normalized ambient density gradient:

$$\epsilon = \frac{1}{\rho_o} \frac{\partial \rho_a}{\partial y} \tag{41}$$

The density gradient inside the cloud is assumed to be less than that in the ambient fluid by a factor $\gamma a_0 / a$, where γ is a coefficient, a_0 is half the final radius of the convective descent cloud (Figure 5), and a is the semi-minor axis of the collapsing cloud. Following these assumptions, the ambient density in the region of the cloud is

$$\rho_a = \rho_0 \, (1 - \epsilon y') = \rho_0 \, (1 - \epsilon \, (a - y)) \tag{42}$$

and the density inside the cloud is

$$\rho = \rho_0 \left(1 - \gamma \frac{a_0}{a} \varepsilon y'\right) = \rho_0 \left(1 - \gamma \frac{a_o}{a} \varepsilon (a-y)\right) \tag{43}$$

where y and y' are as defined in Figure 6. These density profiles are illustrated in Figure 5b.

The centroid of the collapsing slice of the cloud shown in Figure 5c moves with respect to the centroid of the cloud. Consider the slice (of angular dimension $d\theta$) as a free body and integrate the pressures over the surfaces of the slice to obtain the radial force (acting at the slice centroid) driving the collapse of the slice. The pressures are assumed to be hydrostatic. The pressure on the rounded external surface of the slice is simply the pressure in the ambient fluid, $p_a(y)$, and it is integrated over the projected area as shown in Figure 6.

$$F_{ext} = \int_{y=0}^{y=a} p_a(y)\, r(y)\, d\theta\, dy \tag{44}$$

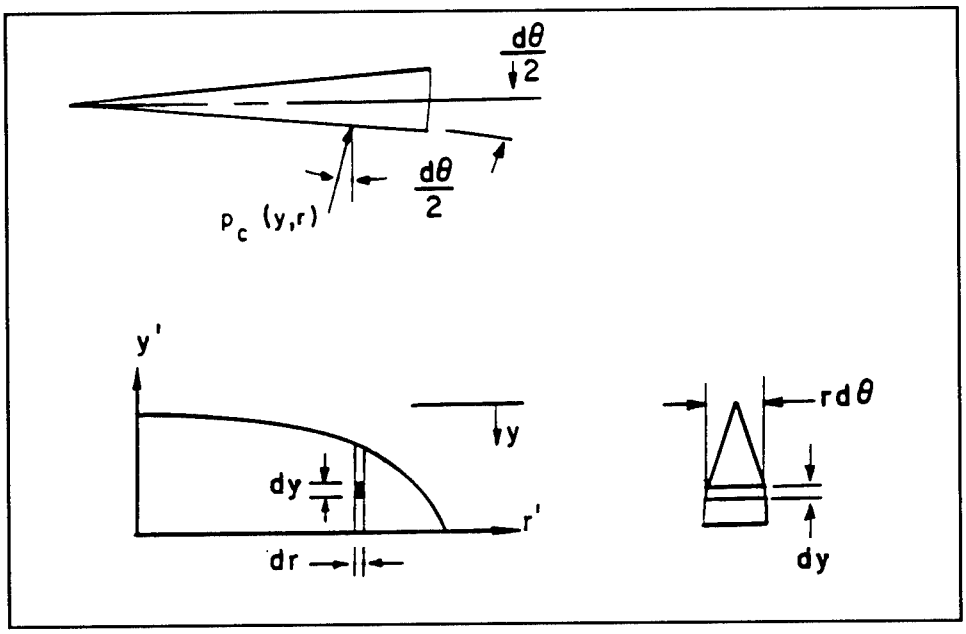

Figure 6. Slice of collapsing cloud, showing integration elements for determining the driving force of collapse (from Brandsma and Divoky (1976))

The pressure inside the cloud, $p_c(y,r)$, is a function of the vertical and radial position inside the cloud. This pressure is integrated over both side faces of

the slice, and $d\theta$ is assumed small to give an expression for the radially outward directed force:

$$F_{int} = \int_0^b \int_{a(1-R)}^{a} p_c(y,r)\, d\theta\, dr dy \tag{45}$$

where $R = \sqrt{1 - \frac{r^2}{b^2}}$.

Once the integrals (44) and (45) are evaluated and the difference of F_{int} - F_{ext} is taken, the radial force driving collapse is obtained:

$$F_D = \frac{\pi \rho_0 (1 - \gamma \frac{a_0}{a})\, \varepsilon\, g a^3 b}{16}\, d\theta \tag{46}$$

Since $\varepsilon = \frac{1}{\rho_o} \frac{\partial \rho_a}{\partial y}$, the expression may be written as

$$F_D = \frac{\pi}{16} (1 - \gamma \frac{a_0}{a}) (\frac{\partial \rho_a}{\partial y})\, g\, a^3 b \quad d\theta \tag{47}$$

In formulating the inertia of the slice and force-resisting collapse, it is assumed that the horizontal velocities of the elements inside the slice are related to the radial distance, r, from the centroid of the cloud and that the velocity of horizontal deformation is characterized by the velocity of the centroid of the slice segment. The cloud tip velocity due to collapse (which will be called v_1) is linearly related to the slice centroid horizontal velocity by

$$v_1 = \frac{16}{3\pi} \frac{dc}{dt} \tag{48}$$

The forces resisting the collapse of the slice are form drag, D_D, and skin friction drag F_f:

$$D_D = C_{drag}\ \rho_a\ \frac{ab}{4}\ |v_1|\ v_1\ d\theta \tag{49}$$

$$F_f = C_{fric}\ \rho_a\ \frac{b^2}{2a}\ v_1\ d\theta \tag{50}$$

where C_{drag} is the drag coefficient for a wedge and C_{fric} is the friction coefficient for a flat plate, which is a function of the kinematic viscosity (Hoerner, 1965).

The horizontal inertia of the cloud slice is the time rate of change of the product of its mass and the velocity of the slice centroid:

$$I = \frac{d}{dt}\left(\rho\ \frac{\pi ab^2}{16}\ v_1\right) d\theta \tag{51}$$

The dynamic equation is formulated as the summation of the external forces acting on the slice which is equated to the inertia.

$$I = F_D - D_D - F_f \tag{52}$$

The integral of Equation 52 over one time step is used to determine the value of v_1 at the end of the time step with $d\Theta$ canceling out of all terms.

The effects of entrainment on mass, momentum, and buoyancy have been considered previously. Entrainment also influences the shape of the cloud cross section, which is assumed to remain symmetric. The rate of volume increase of the cloud due to entrainment is assumed to be accounted for by an increment in the tip velocity with the vertical dimension of the cloud held constant. This increment will be called v_2. The velocity of the slice tip of the collapsing and entraining cloud is:

$$\frac{db}{dt} = v_1 + v_2 \tag{53}$$

Equation (34),as it stands, accounts only for the gross amount of mass entrained. It may be rewritten under the assumptions of constant cloud density and constant vertical dimension during each integration step to describe how entrainment adds to the growth of *b*:

$$v_2 = \frac{E\rho_a - \sum_i S_i \rho_i}{\rho \frac{8}{3} \pi ab} \tag{54}$$

Several additional equations are used for:

Momentum

$$\vec{M} = C_M \rho \frac{4}{3} \pi ab^2 \vec{U} \tag{55}$$

Buoyancy force

$$F = \frac{4}{3} \pi ab^2 g(\rho - \rho_a) \tag{56}$$

Drag force in the x-direction

$$D_x = \frac{1}{2} \rho_a C_{D_3} \pi ab \, |\vec{U} - \vec{U_a}| \, (u - u_a) \tag{57}$$

Drag force in the y-direction

$$D_y = \frac{1}{2} \rho_a C_{D_4} \pi b^2 \, |\vec{U} - \vec{U_a}| \, v \tag{58}$$

Drag force in the z-direction

$$D_z = \frac{1}{2} \rho_a C_{D_3} \pi ab^2 \, |\vec{U} - \vec{U_a}| \, (w - w_a) \tag{59}$$

Buoyancy

$$B = \frac{4}{3}\pi ab^2(\rho_a(0) - \rho) \tag{60}$$

Solid volume of the i^{th} component

$$P_i = \frac{4}{3}\pi ab^2 C_{si} \tag{61}$$

In the above equations, C_M is an apparent mass coefficient, C_{D_3} is the drag coefficient for a spheroidal wedge, and C_{D_4} is the drag coefficient for a circular plate.

As in the convective descent phase, Equations 34-37 are solved by the forward Euler scheme to yield the time history of the disposal cloud while collapsing in the water column. Initial conditions such as the bulk density and axes of the oblate spheroid are provided from the last time step of the convective descent phase.

Dynamic Collapse on Bottom

As previously noted, the convective descent and water column collapse phases are essentially the same as developed by Koh and Chang (1973) and virtually all of the discussion presented, with the exception of the discussion on insertion speed, has been taken from Brandsma and Divoky (1976). However, the manner in which collapse of the disposal cloud is treated when the bottom is encountered during convective descent is completely different.

Bottom collapse in STFATE is computed from a conservation of energy concept. When the cloud strikes the bottom, it possesses a certain amount of potential energy which can be computed since the mass of the cloud and the location of its centroid are known. In addition, the kinetic energy of the impacting cloud can be computed since its velocity is known. Thus, the total energy of the cloud at the moment of impact is known. This energy is then available to drive the resulting bottom collapse or surge.

A basic assumption is that the bottom collapsing cloud is one-half of an ellipsoid. If the bottom is flat, the cloud becomes one-half of an oblate spheroid. From Figure 7, the general equation of an ellipsoid is

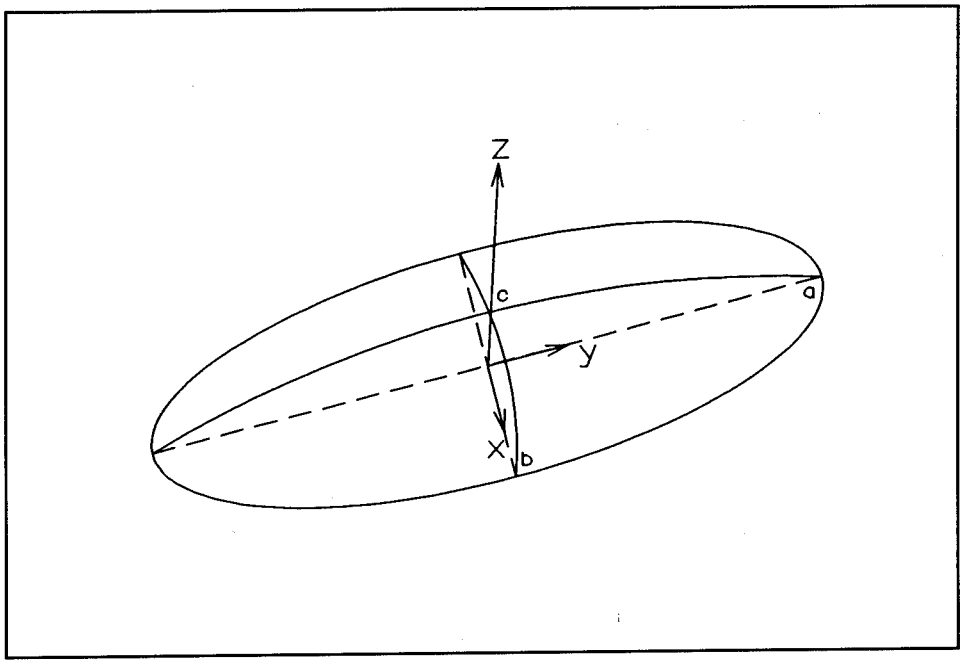

Figure 7. Bottom collapse

$$\left[\frac{x}{b}\right]^2 + \left[\frac{y}{a}\right]^2 + \left[\frac{z}{c}\right]^2 = 1 \tag{62}$$

The kinetic energy of the collapsing cloud can be written as

$$KE = \int_V \int \int \frac{1}{2} \rho (u^2 + v^2 + w^2)\, dV \tag{63}$$

where ρ is the cloud density, (u,v,w) represent the speed of any part of the cloud along the (x,y,z) axes, respectively, and V is the volume of the cloud. Expressions for (u,v,w) can be deduced by integrating Equation 62 with respect to time, yielding

$$\left[\frac{x}{b^2}\right]\dot{x} - \left[\frac{x^2}{b^3}\right]\dot{b} + \left[\frac{y}{a^2}\right]\dot{y} - \left[\frac{y^2}{a^3}\right]\dot{a} + \left[\frac{z}{c^2}\right]\dot{z} - \left[\frac{z^2}{c^3}\right]\dot{c} = 0 \tag{64}$$

Since, by definition, $u = \dot{x}$, $v = \dot{y}$, and $w = \dot{z}$, for Equation 64 to be satisfied the following holds:

$$u = \frac{x}{b}\dot{b} \tag{65}$$

$$v = \frac{y}{a}\dot{a} \tag{66}$$

$$w = \frac{z}{c}\dot{c} \tag{67}$$

Substituting Equations 65-67 into Equation 63 yields the following expression for the kinetic energy:

$$KE = \frac{1}{2}\rho \left\{ \left[\frac{\dot{b}}{b}\right]^2 \iiint_V x^2\, dV + \left[\frac{\dot{a}}{a}\right]^2 \iiint_V y^2\, dV + \left[\frac{\dot{c}}{c}\right]^2 \iiint_V z^2\, dV \right\} \tag{68}$$

Now consider the evaluation of the general expression

$$\iiint_V x^n\, dV = \int_o^b x^n A\, dx \tag{69}$$

where A is the cross-section area in the yz plane. Considering cross-sections in the xz and xy planes, the following equations for an ellipse can be written:

$$\left[\frac{x}{b}\right]^2 + \left[\frac{z}{c}\right]^2 = 1 \tag{70}$$

$$\left[\frac{x}{b}\right]^2 + \left[\frac{y}{a}\right]^2 = 1 \tag{71}$$

In addition, the area can be written as

$$A = \frac{\pi}{4} yz \tag{72}$$

Solving Equation 70 for z and Equation 71 for y and substituting into Equation 72, yields

$$A = \frac{\pi}{4} ac \left[1 - \left[\frac{x}{b}\right]^2\right] \tag{73}$$

Substituting Equation 73 into Equation 69 and evaluating the resulting integrals yields

$$\int\int\int_V x^n \, dV = \frac{\pi}{4} acb^{n+1} \left[\frac{1}{n+1} - \frac{1}{n+3}\right] \tag{74}$$

Using Equation 74 to evaluate the integrals in Equation 68 and now letting V $= \frac{2}{3} \pi abc$ be the volume of a half ellipsoid, the kinetic energy for a quadrant of the half ellipsoid becomes

$$KE = \frac{1}{10} \rho V (\dot{b}^2 + \dot{a}^2 + \dot{c}^2) \tag{75}$$

An expression for the potential energy can be derived as follows. Considering Figure 8, the total potential energy of the surrounding ambient fluid and the collapsing cloud is

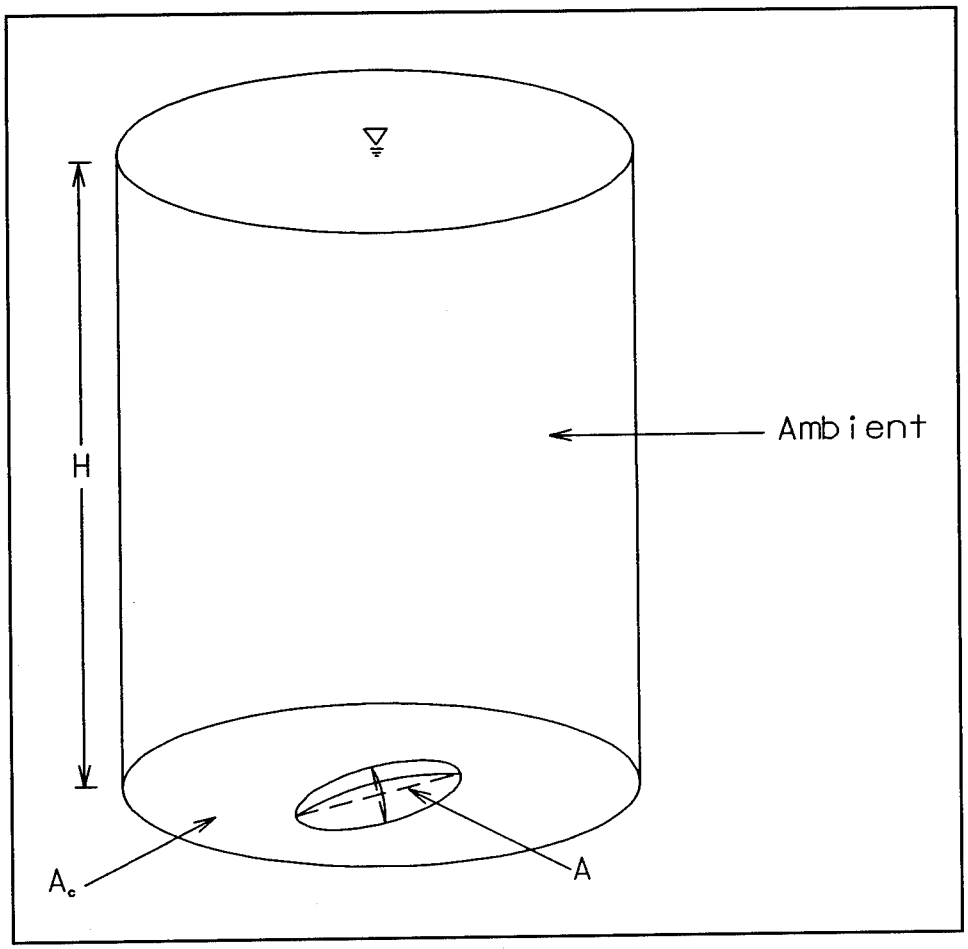

Figure 8. Potential energy of bottom cloud

$$PE = \iiint_{V_T} \rho g y \, dV_T \tag{76}$$

where $V_T = A_c H = (A_c - A)H + AH$

Equation (76) can now be written as

$$PE = \iiint_{(A_c - A)H} \rho g y \; dV_1 + \iiint_{AH} \rho g y \; dV_2 \tag{77}$$

The second integral in Equation 77 can be written as

$$\int_{AH}\int\int \rho g y\, dV_2 = \int_{A}\int \left[\rho g \int_{0}^{a} y\,dy + \rho_a g \int_{a}^{H} y\,dy\right] dA$$
$$= \int_{A}\int \left[(\rho-\rho_a) g \int_{0}^{a} y\,dy\right] dA$$
$$+ \int_{A}\int \left[\rho_a g \int_{o}^{H} y\,dy\right] dA \qquad (78)$$

or

$$PE = \int_{A_c H}\int\int \rho_a g y \; dV_3 + \Delta\rho g \int_{Aa}\int\int y \; dV \qquad (79)$$

If the free surface isn't moving, the first integral above is a constant. Equation 74 can be used to evaluate the second integral, yielding the following expression for the potential energy of a quadrant of the half ellipsoid.

$$PE = \frac{3}{8} \Delta\rho g V a + constant \qquad (80)$$

Since only changes in potential energy influence the dynamics of the collapsing cloud, the constant does not need to be evaluated.

Given that the change in the total energy of the cloud, which is the sum of the kinetic and potential energies, is equal to work done by the cloud, the following expression holds:

$$\Delta KE + \Delta PE = WORK \qquad (81)$$

What is desired are expressions for the time rate of change of a, b and c.

Assuming that

$$\dot{c} = \left[\frac{b}{c}\right] \dot{b} \tag{82}$$

and substituting into Equation 75, yields

$$KE = \frac{1}{10} \rho \forall \left[(\dot{b})^2 + (\dot{a})^2 + \left[\frac{b}{c}\right]^2 (\dot{b})^2\right] \tag{83}$$

Since the time rate of change of the volume of the half ellipsoid is the rate of entrainment of ambient fluid, Q_e, the following expression can be derived:

$$\dot{a} = a \left[\frac{Q_e}{\forall} - \frac{\dot{b}}{b} - \frac{\dot{c}}{c}\right] \tag{84}$$

Substituting Equation 84 into Equation 83 yields the following equation from which the change of b each time step can be determined.

$$\left[1 + \frac{b^2}{c^2} + \frac{a^2}{b^2} + \frac{2a^2}{c^2} + \frac{a^2b^2}{c^4}\right] \left[\frac{\Delta b}{\Delta t}\right]^2 - \frac{2Q_e}{\forall} \left[\frac{1}{b} + \frac{b}{c^2}\right] \left[\frac{\Delta b}{\Delta t}\right] = \frac{10KE}{\rho \forall} - \frac{a^2 Q_e^2}{\forall^2} \tag{85}$$

Once Δb is determined, the change in c is determined from Equation 82 and the change in a from Equation 84.

The computations proceed in the following manner. At the end of the convective descent phase, the kinetic and potential energies of the cloud are

$$KE = \frac{1}{3} \rho \pi R^3 |\overline{U}|^2 \tag{86}$$

$$PE = \frac{1}{4} \Delta\rho g R^3 a \tag{87}$$

where R is the radius of the hemispherical cloud and $a=b=c=R$ at the initiation of collapse. The exception is when disposal takes place in shallow water. In that case, a is set to be the distance from the bottom of the disposal vessel to the sea bottom and $b=c$ is determined so as to conserve the volume of disposal material.

The potential energy of the cloud changes as the cloud density decreases due to entrainment of ambient fluid and the loss of sediment, as well as, due to the height of the centroid of the cloud decreasing as the cloud spreads over the bottom. The change in kinetic energy is computed from Equation 81 once the work done by the collapsing cloud is quantified.

Work must be done to overcome bottom friction, drag, the production of internal turbulence and setting the ambient fluid in motion. The contribution to the work term in Equation 81 due to bottom friction, W_f, is

$$W_f = \frac{1}{4} \rho C_{fric} \pi b c \left[\left(\frac{db}{dt} \right)^2 + \left(\frac{dc}{dt} \right)^2 \right] \left[\sqrt{\left(\frac{db}{dt} \right)^2 + \left(\frac{dc}{dt} \right)^2} \right] \Delta t \tag{88}$$

The contribution due to drag, W_d, is

$$W_d = \frac{1}{4} \rho_a C_{drag} \pi a \sqrt{b^2 + c^2} \left[\left(\frac{db}{dt} \right)^2 + \left(\frac{dc}{dt} \right)^2 \right] \left[\sqrt{\left(\frac{db}{dt} \right)^2 + \left(\frac{dc}{dc} \right)^2} \right] \Delta t \tag{89}$$

The work required to set the ambient fluid in motion is assumed to be some percent of the existing kinetic energy, with the value being input as a model coefficient. The contribution due to the generation of internal turbulence, W_t, is

$$W_t = \frac{2}{3} \pi abc \rho u*^2 \frac{dv}{dz} \Delta t \tag{90}$$

where the friction velocity, u*, is computed from

$$u* = 0.4 \frac{\sqrt{\left(\frac{db}{dt}\right)^2 + \left(\frac{dc}{dt}\right)^2}}{\ln\left(\frac{a}{2z_o}\right)} \tag{91}$$

where z_o is the height of the bottom roughness. The velocity gradient in Equation 90 is computed from

$$\frac{dv}{dz} = \frac{0.7\sqrt{\left(\frac{db}{dt}\right)^2 + \left(\frac{dc}{dt}\right)^2}}{a} \tag{92}$$

Once the change in kinetic energy is computed, the new kinetic energy is known and the changes in *c*, *a*, and *b* can be determined from Equations 82, 84 and 85, respectively.

Time Steps

The computational time step in both the convective descent and collapse phases is determined internally within STFATE. For the case of a uniform ambient density, the first attempt at setting the time step in the convective descent phase is

$$DT = \frac{0.01 R \left(1 + \frac{\alpha H}{R}\right)^2}{w\sqrt{gR \frac{\Delta\rho}{\rho}}} \tag{93}$$

whereas, if the ambient density is non-uniform

$$DT = \frac{0.01\,\pi\, w}{\left(\sqrt{g\frac{\Delta\rho}{\rho}\,R}\right)\left(\sqrt{\frac{\Delta\rho_a}{\Delta\rho}\,\frac{R}{H}}\right)} \tag{94}$$

If the total number of time steps, ISTEP, in the convective descent phase is less than 100 or more than 200, the computations are reinitialized with the new time step determined from

$$DT_{new} = \frac{(DT)\ (ISTEP)}{150} \tag{95}$$

Up to ten trials are allowed. Extensive testing of STFATE over a wide range of conditions have shown that the computations usually converge within ten trials. If not, results from the 10^{th} trial are used.

If collapse occurs in the water column, the initial time step is computed from

$$DT = \frac{0.001\left\{\left[840\,R^3\sqrt{\frac{g}{\rho}\frac{\partial\rho}{\partial y}}\right]^{0.42857}\right\}^3}{R\left(0.1\sqrt{\frac{g}{\rho}\frac{\partial\rho}{\partial y}}\right)} \tag{96}$$

whereas, if collapse occurs on the bottom, it is set to be that used in the convective descent computations. If the total number of collapse time steps, ISTEPC, is less than 100 or greater than 400, the computations are reinitialized and the new time step is computed from

$$DT_{new} = \frac{(DT)\,(ISTEPC)}{250} \tag{97}$$

Equations 93, 94 and 96 were employed by Koh and Chang (1973).

Bottom Slope

The influence of a bottom slope is to increase the spread of the bottom surge in a downslope direction and to decrease the spread in an upslope direction. Within the idealized framework of a collapsing half ellipsoid, this effect is modeled in the following manner in STFATE.

Consider Figure 9. Slopes *sx1*, *sx2*, *sz1* *sz2* are computed at the four centroids shown by subtracting the depth at the cloud centroid from the depth at the individual centroids. Movement of the four centroids shown due to a slope can then be determined from

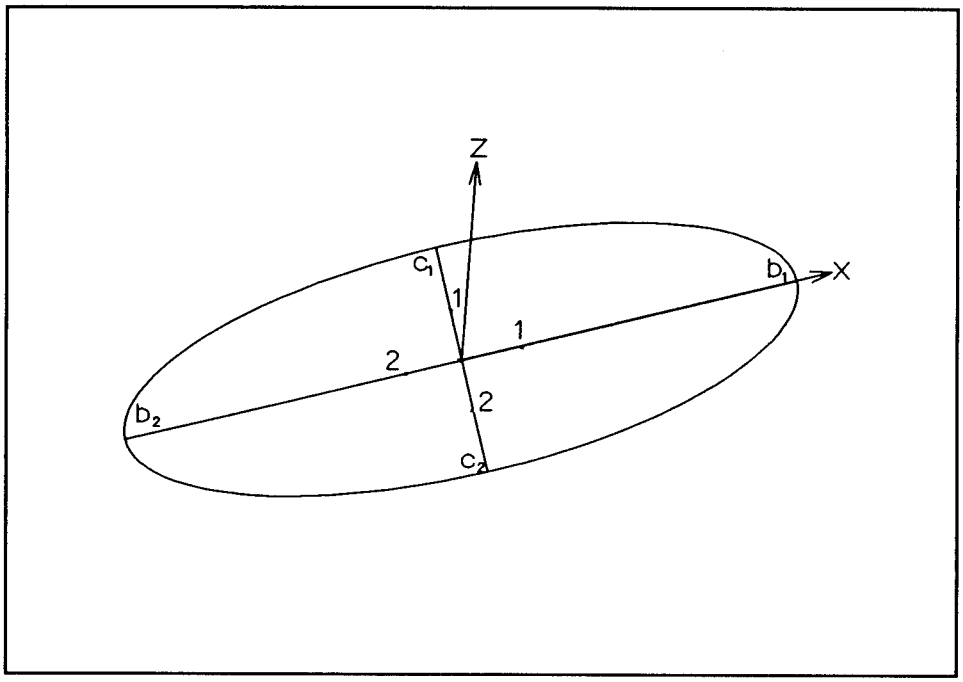

Figure 9. Effect of bottom slope

$$\frac{du_1}{dt} = \frac{\Delta\rho}{\rho} g \sin(sx1) \tag{98}$$

$$\frac{du_2}{dt} = \frac{\Delta\rho}{\rho} g \sin(sx2) \tag{99}$$

$$\frac{dw_1}{dt} = \frac{\Delta\rho}{\rho} g \sin(sz1) \tag{100}$$

$$\frac{dw_2}{dt} = \frac{\Delta\rho}{\rho} g \sin(sz2) \quad (101)$$

Once u_1, u_2, w_1, and w_2 are determined, the change in b_1, b_2, c_1, and c_2 can be determined from

$$\frac{\Delta b_1}{\Delta t} = \frac{8}{3} u_1 \quad (102)$$

$$\frac{\Delta b_2}{\Delta t} = \frac{8}{3} u_2 \quad (103)$$

$$\frac{\Delta c_1}{\Delta t} = \frac{8}{3} w_1 \quad (104)$$

$$\frac{\Delta c_2}{\Delta t} = \frac{8}{3} w_2 \quad (105)$$

The contribution to the bottom spreading as a result of bottom slope then becomes

$$\Delta b = \Delta b_1 + \Delta b_2 \quad (106)$$

$$\Delta c = \Delta c_1 + \Delta c_2 \quad (107)$$

Since the time rate of movement of each of the four centroids is equal to the speeds determined in Equations 98-101, the new locations of the four centroids can be determined. The new location of the total cloud centroid is then determined as an average of the locations of the individual centroids.

Disposal at Dispersive Sites

In the earlier disposal model work, there was no mechanism for keeping material from depositing, and once material was deposited on the bottom it remained there. Thus, at dispersive sites, model results were questionable. In STFATE, a critical shear stress for deposition is specified for each sediment fraction. A computed bottom shear stress is then compared to the critical value to determine if suspended material can be deposited.

If the bottom shear stress is affected only by currents and no waves are present, it is computed from the following expression based upon the assumption of a log profile.

$$\tau_b = \rho_a \frac{0.4\sqrt{u_a^2 + w_a^2}}{\ln\left(\frac{z}{z_o}\right)} = \rho_a u_*^2 \tag{108}$$

where (u_a, w_a) are the components of the ambient velocity, z is the height at which (u_a, w_a) are determined, e.g. 1 m, and z_o is the bottom roughness, e.g., 1 mm. u_* is the friction velocity and becomes u_{*_o} if waves are present.

If waves are present at the disposal site, the following approach taken from Madsen and Wikramanayake (1991) is used. With this approach, the ambient current angle, wave amplitude, wave period, and an initial value for the wave-current angle, wc_o, must be input. The wave-current friction factor, f_{wc}, is computed first from

$$\frac{1}{\sqrt{f_{wc}}} + \log_{10}\left(\frac{1}{4\sqrt{f_{wc}}}\right) = \log_{10}\left(\frac{A_b}{30z_o}\right) + 0.1 \tag{109}$$

if $A_b/(30\ z_o) > 1000$, where A_b is the wave amplitude. However, if $A_b/(30z_o) < 1000$, the following expression is employed.

$$f_{wc} = \exp\left\{5.2\left(\frac{A_b}{30z_o}\right)^{-0.19} - 6.1\right\} - 0.24\left(\frac{A_b}{30z_o}\right)^{-1.2} \tag{110}$$

The next step involves an iteration for the current friction velocity and the wave-current angle. The initial guess for the current friction velocity is u_{*_o}. As noted, the initial guess for the current-wave angle is input. The following iteration involving Equations 113 and 116 is then performed and continues until the values of the current friction velocity and wave-current angle, wc, converge, i.e.,

$$\frac{u_{*_i}}{u_{*_{i-1}}} > 0.99 \tag{111}$$

$$\frac{wc_i}{wc_{i-1}} > 0.99 \tag{112}$$

where i is the iteration number. The procedure is as follows. First compute I1 from

$$I1 = \left(\frac{u_{*_{i-1}}}{0.4}\right)\left\{\ln\left(\frac{z\,u_{*_{i-1}}}{0.64\,u_{*w}}\right) + 1.0 + \left(\frac{1.25\,u_{*_{i-1}}}{u_{*w}}\right)\left(\ln\left(\frac{0.8}{\zeta}\right) - 1.0\right)\right\} \tag{113}$$

where

$$u_{*_w} = A_b\,P_w\sqrt{\frac{f_{wc}}{2.0}} \tag{114}$$

$$\zeta = \frac{z_o}{30\,\dfrac{0.4\,u_{*_w}}{P_w}} \tag{115}$$

and P_w is the input wave period. Then compute I2 from

$$I2 = \left(\frac{u_{*_{i-1}}}{0.4}\right)\left(\frac{0.53\,u_{*_{i-1}}}{(1.0 - \zeta)\,u_{*_w}}\right)\left[\ln\left(\frac{0.8}{\zeta}\right) - 0.78 + \zeta\right] \tag{116}$$

The new estimates for the current friction velocity, u_{*_i}, and the wave-current angle, wc_i, at the i-th iteration are then computed from

$$u_{*_i} = u_{*_{i-1}} \left(\frac{\sqrt{u_a^2 + w_a^2}}{\lambda} \right) \tag{117}$$

where

$$\lambda = \sqrt{(I1 - I2)^2 \cos^2(wc_{i-1}) + I1^2 \sin^2(wc_{i-1})} \tag{118}$$

and

$$wc_i = wc_{i-1} + (wc_o - \alpha) \tag{119}$$

where

$$\alpha = TAN^{-1} \left[TAN(wc_{i-1}) \frac{I1}{I1 - I2} \right] \tag{120}$$

With the convergence of u_{*_i} and wc_i, the total bottom shear stress is then computed from

$$\tau_b = \left\{ \left[\rho_a u_{*_w}^2 \cos(P_w t) + \rho_a u_{*_i}^2 \cos(wc_i) \right]^2 + \left[\rho_a u_{*_i}^2 \sin(wc_i) \right]^2 \right\}^{1/2} \tag{121}$$

The shear stress computed from either Equation 108 or Equation 121 is then compared to the critical shear stress for deposition to determine if a particular sediment fraction deposits.

Transport-Diffusion Phase

At most disposal sites, the convective descent and dynamic collapse phases only last on the order of a few minutes. When the rate of spreading of the collapsing cloud becomes less than an estimated rate of spreading due to turbulent diffusion, the collapse phase is terminated and the "longer" term transport-diffusion phase is initiated. In this phase, material in suspension is

transported and diffused by the ambient current while undergoing settling. Of course any non-sediment constituent being modeled is also transported and diffused.

A basic assumption in the transport-diffusion phase is that material (or constituent) concentrations can be determined from a superposition of small clouds characterized by a normal or Gaussian distribution, i.e.,

$$C = \frac{m}{(2\pi)^{3/2}\sigma_x\sigma_y\sigma_z} \exp\left\{-1/2\left[\frac{(x-x_o)^2}{\sigma_x^2} + \frac{(z-z_o)^2}{\sigma_z^2} + \frac{(y-y_o)^2}{\sigma_y^2}\right]\right\} \quad (122)$$

where

m = volume of solids in the cloud, ft^3
$\sigma_x,\sigma_y,\sigma_z$, = standard deviations, ft
x,y,z = spatial coordinates, ft
x_o,y_o,z_o = coordinates of cloud centroid, ft

These clouds are formed as material is stripped away during the descent of the convecting clouds as well as during the collapse phase. For collapse in the water column, small clouds are formed as material settles from the collapsing cloud. However, during collapse on the bottom, laboratory experiments by Johnson, et al. (1993) as well as field data collected at Mobile, AL by Kraus (1991) imply that fine material is also lost to the water column at the top of the collapsing cloud.

At the end of each time-step, each cloud is advected horizontally by the input velocity field. The new position of the cloud centroid is determined by

$$x_{o_{new}} = x_{o_{old}} + u \cdot \Delta t \quad (123)$$

$$z_{o_{new}} = z_{o_{old}} + w \cdot \Delta t \quad (124)$$

where

u,w = input ambient velocities, fps
Δt = long-term time-step, sec

In addition to the advection or transport of the cloud, the cloud grows both horizontally and vertically as a result of turbulent diffusion. The horizontal

diffusion is based upon the commonly assumed four-thirds power law. Therefore, the diffusion coefficient, $K_{x,z}$, (up to a maximum value of 100 ft^2/s) is given as

$$K_{x,z_{new}} = A_L L^{4/3} \tag{125}$$

where A_L is an input dissipation parameter and L is set equal to four standard deviations. As illustrated in Figure 2.4 of the report by Brandsma and Divoky (1976), a value of 100 ft^2/sec for the horizontal diffusion coefficient corresponds to a length scale of 10^3-10^4 ft. With the computational grid cell typically being on the order of 100-500 ft, a length scale greater than 1,000 ft would normally be associated with mean flow rather than turbulence. Thus, restricting the diffusion coefficient to be less than 100 ft^2/sec is reasonable.

Horizontal growth is achieved by employing the Fickian expression

$$\sigma_{x,z} = (2K_{x,z}t)^{1/2} \tag{126}$$

where

$\sigma_{x,z}$ = a standard deviation
t = time since formation of the cloud

From Equation 126.

$$\frac{d\sigma_{x,z}}{dt} = K_{x,z}\,(2K_{x,z}t)^{-1/2} \tag{127}$$

and thus,

$$\sigma_{x,z_{new}} = \sigma_{x,z_{old}} + \frac{K_{x,z_{new}}}{\sigma_{x,z_{old}}}\,\Delta t \tag{128}$$

where

$\sigma_{x,z_{new}} = \sigma_{x,z}$ at the current time step
$\sigma_{x,z_{old}} = \sigma_{x,z}$ at the previous time step

In a similar manner, the vertical growth is written as

$$\sigma_{y_{new}} = \sigma_{y_{old}} + \frac{K_y}{\sigma_{y_{old}}} \Delta t \tag{129}$$

where K_y is a function of the stratification (including the effect of the total suspended sediment) of the water column. The maximum value of K_y is input as a model coefficient and occurs when the water density is uniform.

If long-term output is desired at the end of a particular time-step, the concentration of each solid type is given at each grid point by summing the contribution from individual clouds to yield

$$C_T = (2\pi)^{-3/2} \sum_{i=1}^{N} \frac{m_i}{\sigma_{x_i}\sigma_{y_i}\sigma_{z_i}} \exp\left\{-1/2\left[\frac{(x-x_{o_i})^2}{\sigma_{x_i}^2} + \frac{(y-y_{o_i})^2}{\sigma_{y_i}^2} + \frac{(z-z_{o_i})^2}{\sigma_{z_i}^2}\right]\right\} \tag{130}$$

where N is the number of small clouds of a particular solid type and y (the vertical position at which output is desired) is specified through input data. (x,z) are the horizontal coordinates of a grid point. This approach for the transport-diffusion phase follows the work of Brandsma and Sauer (1983). The surface and all solid boundaries except the bottom are handled by assuming reflection from the boundaries.

In addition to the horizontal advection and diffusion of material, settling of the suspended solids also occurs. Therefore, at each net point the amount of solid material deposited on the bottom and a corresponding thickness are also determined. Since a normal distribution is assumed for material in the small clouds, deposited material is also assumed to take such a distribution horizontally on the bottom. A basic assumption in the model is that once material is deposited on the bottom, it remains there; i.e., neither erosion nor bed-load movement of material is allowed. However, as previously discussed, deposition is prohibited if the computed bottom shear stress exceeds a specified critical shear stress for deposition for each solid fraction. This allows for application at dispersive sites.

The discussion presented above for transport-diffusion of solids also applies to the disposed fluid with its dissolved constituents. The constituents are assumed to be conservative with no further adsorption on or desorption from the solids in the water column or those deposited on the bottom. Computing the resultant time-history of constituent concentration provides information on

the dilution that can be expected over a period of time at the disposal site and enables the computation of mixing zones in water column evaluations.

Ambient Environment

As illustrated in Figure 10, time-invariant velocity profiles that allow for flow reversal can be prescribed. These profiles are applied at each grid point. Another option is to specify a time-invariant, spatially varying depth-averaged velocity. The ambient density profile at the deepest point on the grid must also be prescribed.

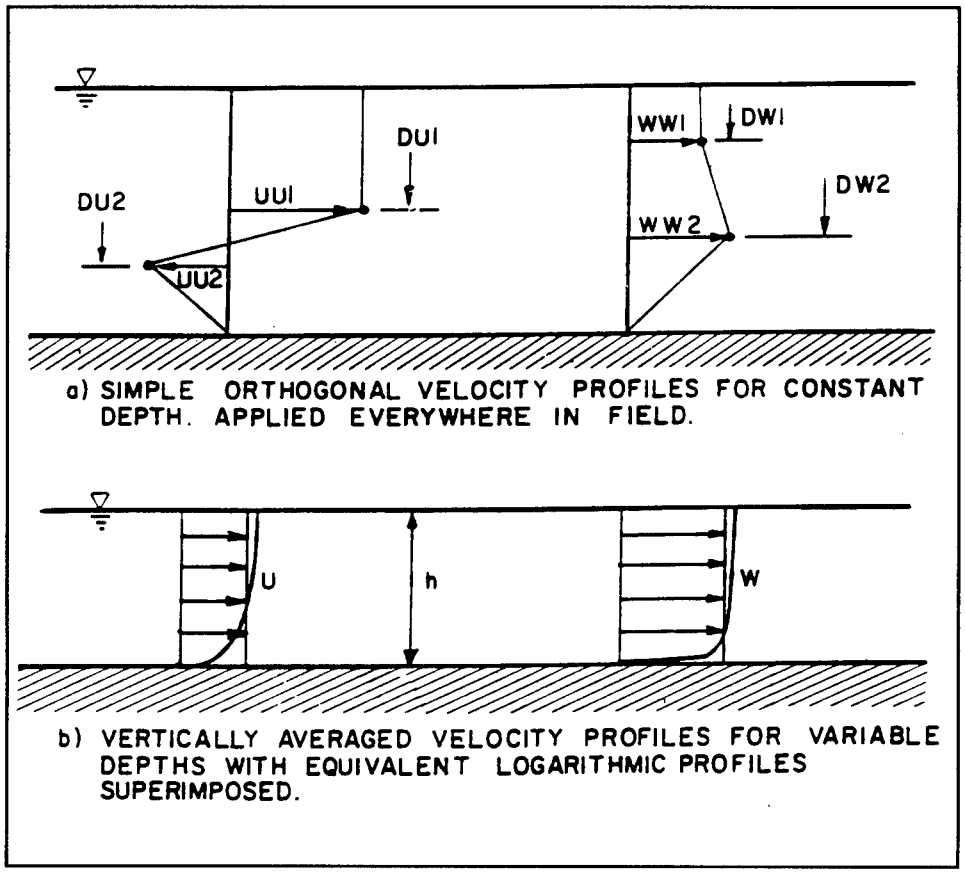

Figure 10. Time invariant velocity profile

Time-Varying Fall Velocities

If a solid fraction is specified as being cohesive, the settling velocity is computed as a function of the suspended sediment concentration of that solid type. The algorithm used is

$$V_s \begin{cases} = 0.000034 \text{ if } C \leq 25 \text{ mg/}\ell \\ = 0.0000225 + 1.6 \times 10^{7} C^{4/3} \text{ if } 25 \leq C \leq 3000 \text{ mg/}\ell \\ = 0.0069 \text{ if } C > 3000 \text{ mg/}\ell \end{cases} \quad (131)$$

where

V_s = settling velocity, fps
C = suspended sediment concentration, mg/ℓ

This algorithm was provided by Teeter (personal communication) of WES.

3 Model Simulations of Laboratory Tests

Large-scale laboratory tests of disposals from a model split-hull barge and a multiple bin vessel are discussed by Johnson, et al. (1993). The tests were conducted in water depths up to 6 ft with the maximum horizontal dimensions of the test facility being 32 ft by 41 ft. Both stationary and moving disposal operations were simulated with disposal materials ranging from essentially pure clay to fine coal. Data collected consisted of bottom deposition areas and depths, suspended sediment samples, and video taping.

Data from these tests helped to guide the model developments described in Part 2 of this report and have also been used to assess the ability of STFATE to accurately simulate disposal of dredged material in open water. Results from seven applications are presented below. Basic information concerning the simulated tests are given in Table 1. For consistency, the test numbers correspond to those reported in Johnson, et al. (1993).

Table 1
Characteristics of Disposal Tests

Test No.	Type Disposal	Water Depth ft	Material	Bulk Density gm/cc
3	Barge	4.5	Sand	1.85
5C	Barge	6.0	Coal	1.15
20	Barge	6.0	Clay	1.13
22	Barge	2.6	Silt	1.06
24	Barge	4.0	Silt	1.14
1H	Hopper	2.0	Silt	1.155
5H	Hopper	4.0	Silt	1.18

As previously discussed, several model coefficients are required. Default values were employed for most. However, larger values were required for the descent and collapse entrainment coefficients. In addition, it was found that better results were obtained if none of the kinetic energy was expended to set

the ambient fluid in motion. Values for all coefficients are given in Table 2. The same values were used in all simulations

Table 2
Model Coefficients used in Simulations

Coefficient	Description	Value
α_o	Descent Entrainment	0.60
β	Settling	0.0
C_m	Apparent Mass	1.0
C_D	Descent Drag	1.0
C_{DRAG}	Collapse Drag	0.5
C_{FRIC}	Fluid Friction	0.004
α_c	Collapse Entrainment	0.03
FRICTN	Bottom Friction	0.01
λ	Horizontal Diffusion Parameter	0.00001
AKYO	Unstratified Vertical Diffusion Coeff	NA
CSTRIP	Stripping	0.003

An extremely low value was used for the horizontal diffusion parameter, λ, because the disposal environment was quiescent. For the same reason, the value of the vertical diffusion coefficient, AKYO, is immaterial. With no ambient velocity, the laminar value for vertical diffusion is used.

Test No. 3

This test was the disposal of sand from a stationary 1:50 scale barge that opened instantaneously. The volume of material released was 0.9 cu ft, representing about 4000 cu yd prototype. The disposal material had a grain size ranging from 0.15 to 0.80 mm. As shown in Table 1, the water depth was 4.5 ft.

Basic data from the disposal test compared with model results are the average descent velocity of the descenting jet or cloud, average rate of spreading of the bottom collapsing cloud, depositional area, and suspended sediment concentrations determined from bottle samples collected at several depths at various locations near the barge at different times. Bottles placed on a pole were opened after the bottom surge front had moved 1 ft past the pole. The locations of the poles containing the sediment bottles are shown in Figure 11. Additional details concerning all tests and the testing program are provided by Johnson, et al. (1993).

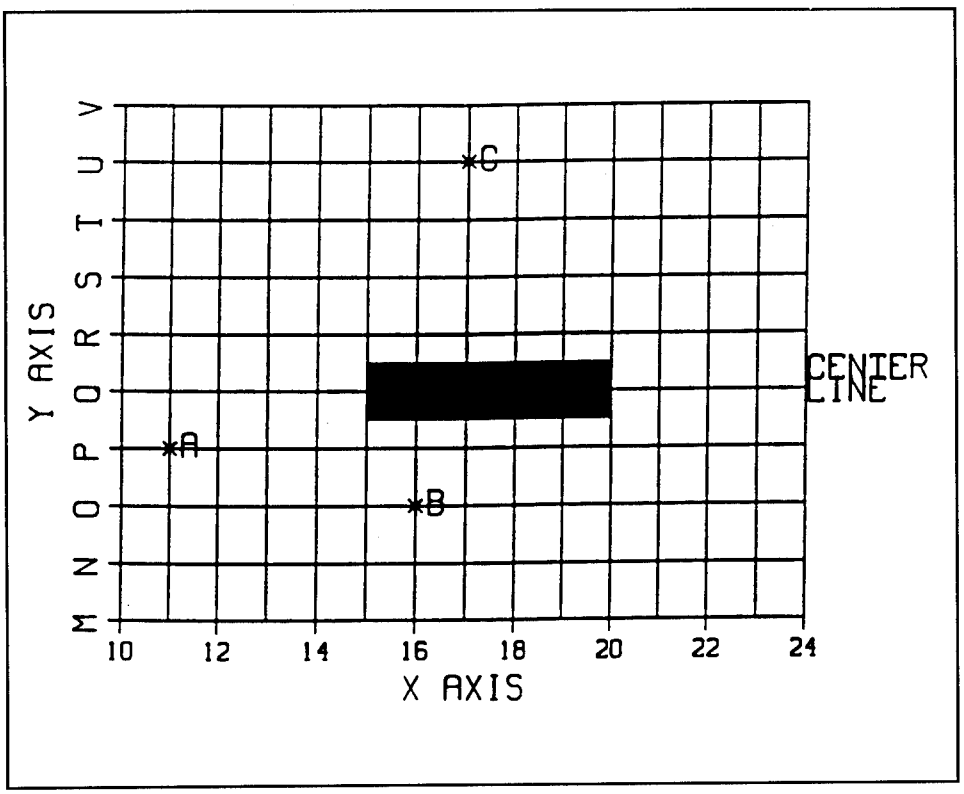

Figure 11. Location of sediment bottles poles for Test No. 3

Data on the convective descent and collapse phases were not available for Test No. 3. However, suspended sediment data were available for comparison with model results. These are presented in Tables 3-4. The suspended sediment concentrations computed by STFATE at various depths at increments of 1 ft from the point of disposal are listed. Measured concentrations are shown in parenthesis and were collected at approximately the locations indicated on the table.

The actual time at which data were collected at Pole B was not recorded, however, based upon timings from other tests it was probably in the 10-15 sec range. Thus, comparisons are shown at 12 and 15 sec. Considering the fact that the manner in which the material leaves the disposal vessel and the timing of pulling the stoppers from the bottles along with the location of the bottles are crucial to the amount of sediment collected in a bottle, the comparison is quite good. An interesting observation is that in some cases the measured concentrations were greater at 6 in. off the bottom than at 3 in. from the bottom. Table 4 illustrates that this behavior was also computed by STFATE.

An inspection of Tables 3-4 shows that the computed concentration field changed significantly from 12 to 15 seconds. This is because the bottom surge is still spreading and also because the material stripped during descent and from the top of the bottom surge has settled 0.3 ft (assuming a fall velocity of 0.1 fps).

Table 3
Comparison of Computed and Measured Suspended Sediment Concentration (mg/ℓ) at Pole B After 12 Seconds

Depth (ft)	Horizontal Position Relative to Point of Disposal (ft)							
	0	1	2	3	4	5	6	7
1.5	3480	5100	31	0	0	0	0	0
			(1)					
2.5	710	1640	270	3	0	0	0	0
			(352)					
3.5	8700	18300	20100	11900	4000	830	110	0
			(17074)					
4.0	7100	13400	17100	15000	9000	3800	1100	210
			(13907)					
4.25	11000	18100	23800	25200	22000	16700	11900	8400

Table 4
Comparison of Computed and Measured Suspended Sediment Concentration (mg/ℓ) at Pole B After 15 Seconds

Depth (ft)	Horizontal Position Relative to Point of Disposal (ft)							
	0	1	2	3	4	5	6	7
1.5	160	240	2	0	0	0	0	0
			(1)					
2.5	690	1460	110	1	0	0	0	0
			(352)					
3.5	6700	14800	14400	630	130	10	0	0
			(17074)					
4.0	6800	14100	16100	10300	3800	770	90	0
			(13907)					
4.25	8400	9700	10900	9600	6400	3600	1900	1200

The measured concentrations are quite sensitive to the time at which the bottled samples were taken since the bottom surge expands similar to a circular torus. Samples taken in the advancing head of the surge (see Figure 12) reveal larger concentrations at greater heights above the bottom than those taken behind the head. Therefore, it is more meaningful for model and measured results to be compared in an average sense over the entire water column rather than focusing on comparisons at a particular point at a particular time. For this reason, the measured concentrations for all tests are presented between concentrations computed at adjacent depths and distances. The measured concentrations should be considered with respect to the four computed values which surrounds them on the tables.

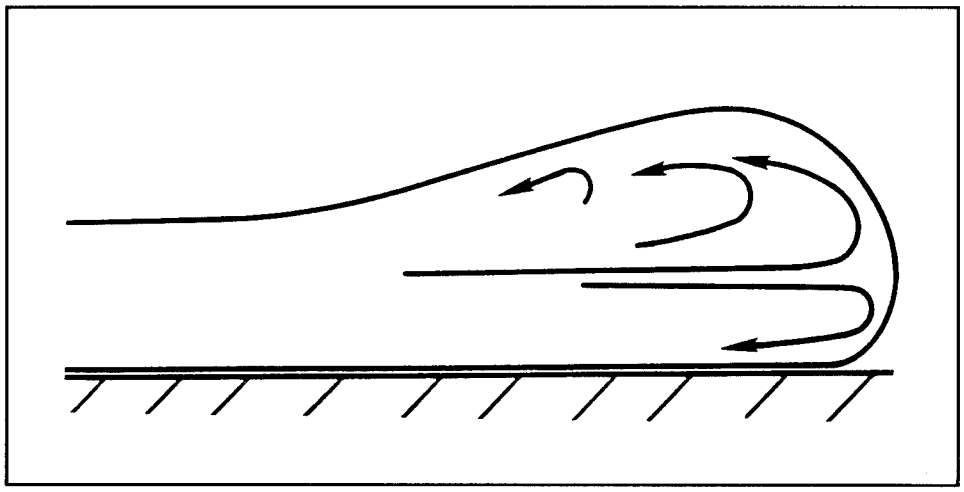

Figure 12. Bottom surge

Test No. 5C

This test was the disposal of crushed coal with a density of 1.3 gm/cc from the model split-hull barge in a water depth of 6 ft. The average descent speed of the disposal cloud was computed to be 0.57 fps. From video tapes of the disposal, the actual descent speed was 0.43 fps. With an entrainment coefficient of 0.60, the disposal material was diluted by a factor of 65 during descent. An entrainment coefficient of 0.60 was estimated from acoustical data collected during a disposal operation near Mobile, FL (Kraus (1991)). Based upon the observed size of the cloud at the moment of bottom impact, a dilution factor of 65 is approximately correct.

The stripping algorithm in STFATE resulted in about 10 percent of the solids being stripped during the descent through 6 ft of water. Although no measurements were taken that can confirm this, it appears to be in line with published figures of 3-5 percent being stripped at disposal sites 100-200 ft deep. The 6 ft water depth scales to a prototype depth of 300 ft. At deeper sites, one would expect a larger percentage of the solids to be stripped. In

addition, the initial concentration of coal was taken to be 50 percent, resulting in a larger stripped quantity.

The average speed of the front of the bottom surge over the first 3-4 ft from the point of disposal was computed by STFATE to be 0.26 fps. Results from the video data show an advancing speed of 0.28 fps.

Suspended sediment comparisons at the locations shown in Figure 13 are presented in Tables 5-6

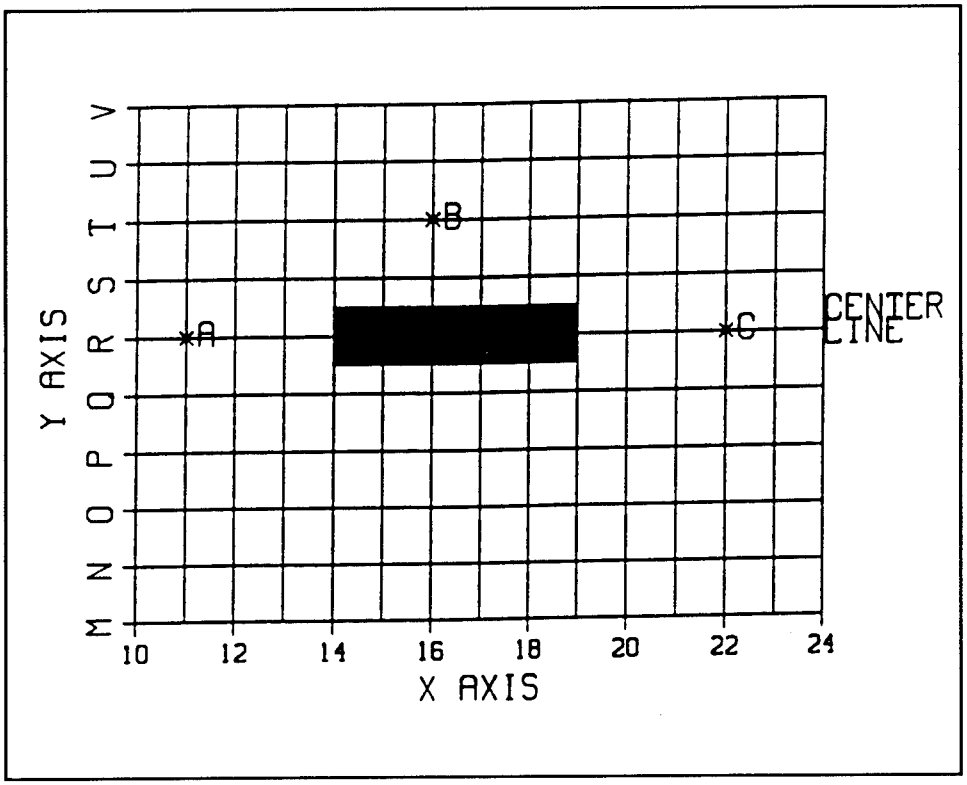

Figure 13. Location of sediment bottles poles for Test No. 5C

Test No. 20

This test was the only disposal conducted with clay material. The disposal occurred from the split-hull barge in 6 ft of water. The averaged descent speed was computed to be 0.55 fps, whereas, the measured speed was 0.67 fps. Approximately 2 percent of the solids are computed to have been stripped from the descenting cloud. This is significantly less than experienced by the crushed coal disposal in Test No. 5C due to the cloud containing less sediment. Stripping of material during descent is related to the concentration of sediment in the descending cloud.

Table 5
Comparison of Computed and Measured Suspended Sediment Concentration (mg/ℓ) at Pole B After 17 Seconds

Depth (ft)	Horizontal Position Relative to Point of Disposal (ft)					
	0	2	4	6	8	10
2.5	425	360	0	0	0	0
		(20)				
3.5	3090	7400	2060	70	0	0
		(5720)				
4.5	500	1100	1100	500	100	10
		(18319)				
5.5	7800	17100	17100	7800	1600	140
		(14137)				
5.75	5500	12100	12000	5400	1100	100

Table 6
Comparison of Computed and Measured Suspended Sediment Concentration (mg/ℓ) at Pole A After 30 Seconds

Depth (ft)	Horizontal Position Relative to Point of Disposal (ft)							
	0	2	4	6	8	10	12	14
			(25)					
2.5	500	230	0	0	0	0	0	0
			(216)					
3.5	2510	5790	1020	15	0	0	0	0
			(2703)					
4.5	660	1580	800	90	2	0	0	0
			(4615)					
5.5	370	710	900	760	430	160	40	0
			(2347)					
5.75	1220	2330	2970	2520	1430	540	140	25

The average speed of the bottom surge over the first couple of feet was computed to be 0.38 fps, whereas, the speed determined from video tapes was 0.57 fps. The reason for the difference is not known. Model and measured bottom surge speeds compared well in most tests. The difference could be due to reduced frictional effects at the bottom.

Suspended sediment concentrations at the locations shown in Figure 14 are presented in Tables 7-8.

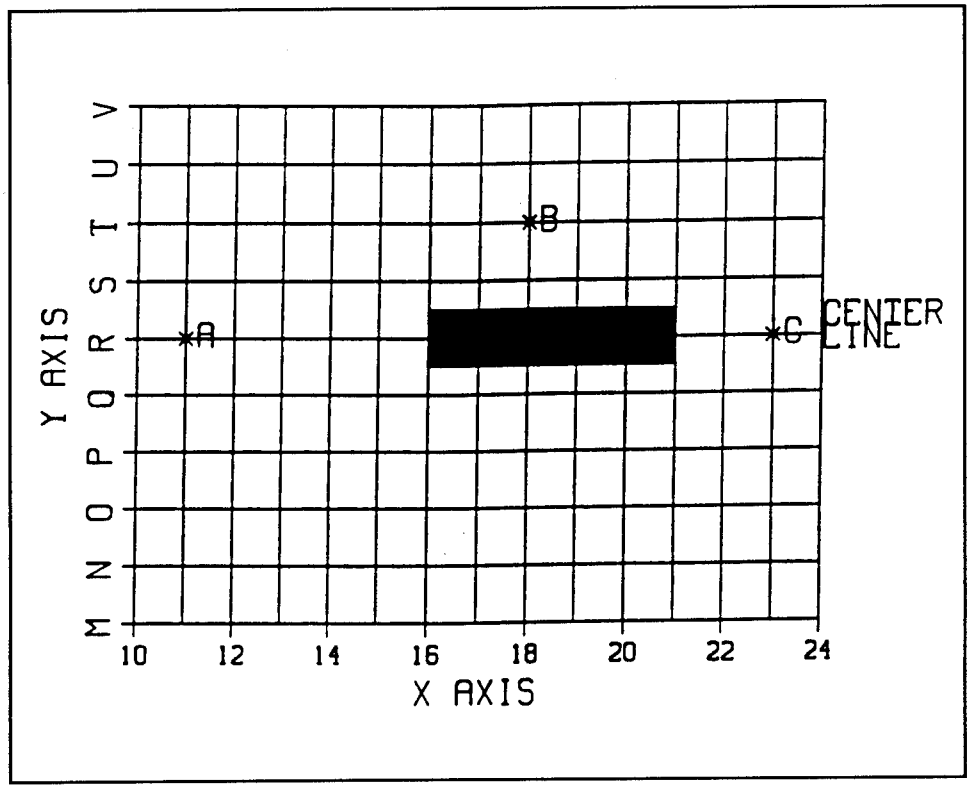

Figure 14. Location of sediment bottles poles for Test No. 20

Model results and measured concentrations compare well, although, the model computes concentrations slightly smaller than those measured in the upper water column.

Bottom deposition was not measurable. However, the general observation that the material covered the entire test area agrees with the model results. Computed depositions greater than 0.05×10^{-5} ft covered an area with a diameter of 32 ft. The maximum deposition thickness was computed to be 3.3×10^{-5} ft.

Table 7
Comparison of Computed and Measured Suspended Sediment Concentration (mg/ℓ) at Pole C After 42 Seconds

Depth (ft)	Horizontal Position Relative to Point of Disposal (ft)							
	0	2	4	6	8	10	12	14
2.5	20	30	0	0	0	0	0	0
3.5	460	1110	420	25	0	0	0	0
4.5	1950	4330	4210	1820	370	35	2	0
				(2079)				
5.5	290	520	690	680	500	275	110	35
5.75	275	470	630	660	540	345	170	70

Table 8
Comparison of Computed and Measured Suspended Sediment Concentration (mg/ℓ) at Pole A After 47 Seconds

Depth (ft)	Horizontal Position Relative to Point of Disposal (ft)							
	0	2	4	6	8	10	12	14
				(68)				
2.5	30	50	2	0	0	0	0	0
				(66)				
3.5	660	1600	650	45	1	0	0	0
				(759)				
4.5	290	640	630	285	60	5	0	0
				(844)				
5.5	300	530	700	690	500	270	115	35
				(1035)				
5.75	450	760	1020	1080	900	590	300	120

Test No. 22

This test was the disposal of a silt slurry with a bulk density of 1.06 gm/cc in 2.6 ft of water from the split-hull barge. The average descent speed was computed to be 1.00 fps, whereas, the measured speed from video tapes was 1.47 fps. Comparisons of descent speed for the greater depth disposals are in

better agreement than those in shallower water which implies that the algorithm for computing the injection speed should be investigated.

The average bottom surge speed over the first couple of feet was computed to be 0.46 fps. Video tape data shows an actual speed of about 0.42 fps.

Computed suspended sediment concentrations at the locations shown in Figure 15 along with the measured concentration placed in parenthesis are presented in Tables 9-11.

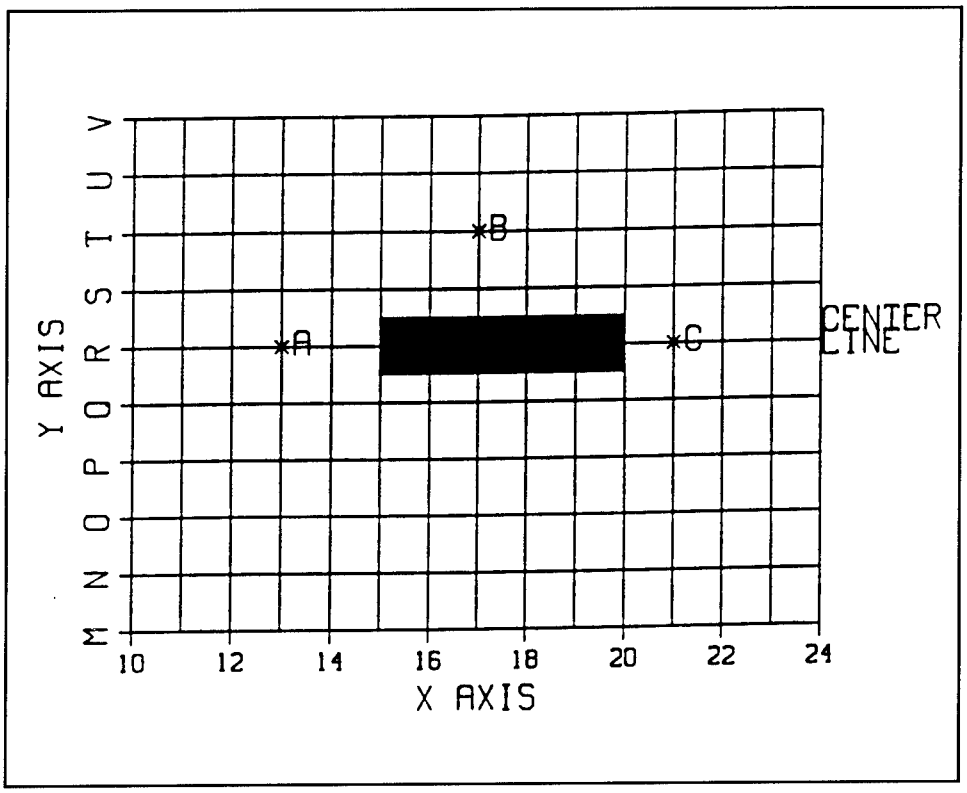

Figure 15. Location of sediment bottles poles for Test No. 22

An inspection of these results reveals that the model underpredicted concentrations in the upper part of the water column as the surge expanded. It should be realized that the exact shape of the bottom surge is not simulated. STFATE assumes that the surge is a collapsing half ellipsoid, whereas, the actual surge is a circular torus. The effect of the torus shape on water column concentrations is approximately accounted for in STFATE by employing an offset Gaussian distribution for the clouds stripped away at the top of the surge. As illustrated in Tables 9-10, this results in better predictions of suspended sediment concentrations in the upper water column closer to the discharge point.

The deposited material covered an area of about 200 ft^2 with an elliptical shape. The computed area of deposition with deposits of greater depth than

Table 9
Comparison of Computed and Measured Suspended Sediment Concentration (mg/ℓ) at Pole B After 12 Seconds

Depth (ft)	Horizontal Position Relative to Point of Disposal (ft)						
	0	1	2	3	4	5	6
0.5	405	275	0	0	0	0	0
			(429)				
1.5	4170	8650	520	0	0	0	0
			(1300)				
2.0	3600	8730	4410	460	10	0	0
			(3306)				
2.25	2310	5100	5040	2250	470	50	5

Table 10
Comparison of Computed and Measured Suspended Sediment Concentration (mg/ℓ) at Pole A After 23 Seconds

Depth (ft)	Horizontal Position Relative to Point of Discharge (ft)					
	0	1	2	3	4	5
0.5	210	170	0	0		0
					(288)	
1.5	3380	6880	360	360		0
					(615)	
2.0	3430	8280	2520	2520	0	0
					(388)	
2.25	2530	5760	5070	1720	230	10

0.03 x 10^{-3} ft was about 150 ft^2, with the greatest deposition depth being 1.9 x 10^{-3} ft.

Test No. 24

This test was the disposal of a silt slurry with a density of 1.14 gm/cc in 4.0 ft of water from the model split-hull barge. The average descent speed

Table 11
Comparison of Computed and Measured Suspended Sediment Concentration (mg/ℓ) at Pole C After 37 Seconds

Depth (ft)	Horizontal Position Relative to Point of Discharge (ft)					
	0	1	2	3	4	5
0.5	45	50	0	0	0	0
				(149)		
1.5	195	370	20	0	0	0
				(423)		
2.0	3520	8440	2260	70	0	0
				(609)		
2.25	2830	6760	3960	730	75	5

was computed to be 0.80 fps, whereas, the measured speed was 0.73 fps. The dilution factor was computed to be about 20 with approximately 1.5 percent of the solids stripped during descent.

The average speed of the front of the bottom surge over the first couple of feet was computed to be 0.42 fps with the measured speed being 0.28 fps. As previously noted, material can leave the disposal vessel in a nonuniform fashion rather than as a single cloud formed instantaneously. This can have an impact on the speed of the surge during its early development.

A comparison of computed and measured suspended sediment concentrations at the locations shown in Figure 16 is given in Tables 12-14.

Unlike some of the previous comparisons, these results show better agreement away from the disposal point. Again, the exact reason is not known but as previously discussed, the time of the release of the bottle corks and the manner in which material is released play a major role in the amount of material captured by an individual bottle.

The observed area of deposition was about 225 ft^2 and was elliptical in shape. The computed area of deposition within which the depth exceeded 0.21×10^{-3} ft was about 200 ft^2 with the maximum depth being 1.60×10^{-3} ft. Depths less than 0.21×10^{-3} ft were outside the computational grid.

Test No. 1H

This test was the disposal of a silt slurry from a 1:50 scale model hopper vessel containing 6 bins. The bulk density was 1.155 gm/cc and the total

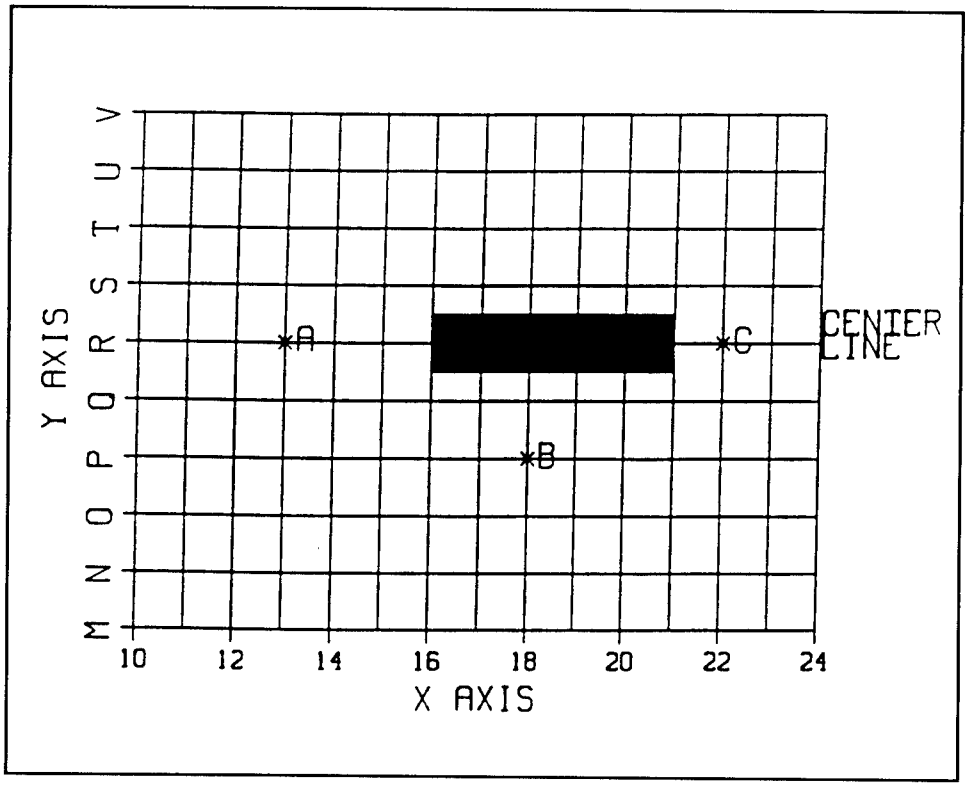

Figure 16. Location of sediment bottles poles for Test No. 24

volume was 1.68 ft^3. Disposal occurred in 2.0 ft of water with pairs of bins opened in sequence. With the disposal occurring in such shallow water, impact with the bottom occurred almost instantaneously. The average speed of the surge front over the first 2-3 ft was 0.44 fps with the average measured speed being 0.42 fps.

Comparisons of computed and measured suspended sediment concentrations at the locations shown in Figure 17 are given in Tables 15-16. In these tables, four rows of computed concentrations are presented at each depth with the first row lying along the center line of the vessel.

Test No. 5H

This test was similar to Test 1H. However, the disposal was in 4.0 ft of water and the bulk density of the silt slurry was 1.18 gm/cc. The average computed descent speed was 1.10 fps, whereas, the measured speed was 1.48 fps. The average speed of the bottom surge over the first 2-3 ft was computed to be 0.47 fps with the average measured speed being 0.45 fps.

Comparisons of computed and measured suspended sediment concentrations at locations shown in Figure 18 are presented in Tables 17-18. As in

Table 12
Comparison of Computed and Measured Suspended Sediment Concentration (mg/ℓ) at Pole B After 12 Seconds

Depth (ft)	Horizontal Position Relative to Point of Discharge (ft)								
	0	1	2	3	4	5	6	7	8
1.0	640	870	5	0	0	0	0	0	0
2.0	490	1160	490	55	0	0	0	0	0
			(562)						
3.0	1330	2870	2990	1550	410	55	5	0	0
			(1544)						
3.5	1440	2580	3410	3310	2370	1250	490	150	30
			(1932)						
3.75	2530	4280	5740	6110	5140	3430	1820	760	250

Table 13
Comparison of Computed and Measured Suspended Sediment Concentration (mg/ℓ) at Pole A After 21 Seconds

Depth (ft)	Horizontal Position Relative to Point of Discharge (ft)								
	0	1	2	3	4	5	6	7	8
1.0	355	500	0	0	0	0	0	0	0
					(129)				
2.0	165	380	50	0	0	0	0	0	0
					(918)				
3.0	1930	4000	4550	2890	1030	200	20	0	0
					(2353)				
3.5	1730	3190	4160	3820	2490	1150	370	90	0
					(1900)				
3.75	680	1020	1350	1590	1660	1530	1260	920	590

Table 14
Comparison of Computed and Measured Suspended Sediment Concentration (mg/ℓ) at Pole C After 35 Seconds

Depth (ft)	Horizontal Position Relative to Point of Discharge (ft)								
	0	1	2	3	4	5	6	7	8
1.0	65	95	0	0	0	0	0	0	0
				(49)					
2.0	190	410	40	0	0	0	0	0	0
				(868)					
3.0	2230	4970	4780	2030	380	30	0	0	0
				(1206)					
3.5	1440	2740	3490	2980	1710	650	170	30	0
				(912)					
3.75	1230	2080	2770	2920	2460	1690	980	520	280

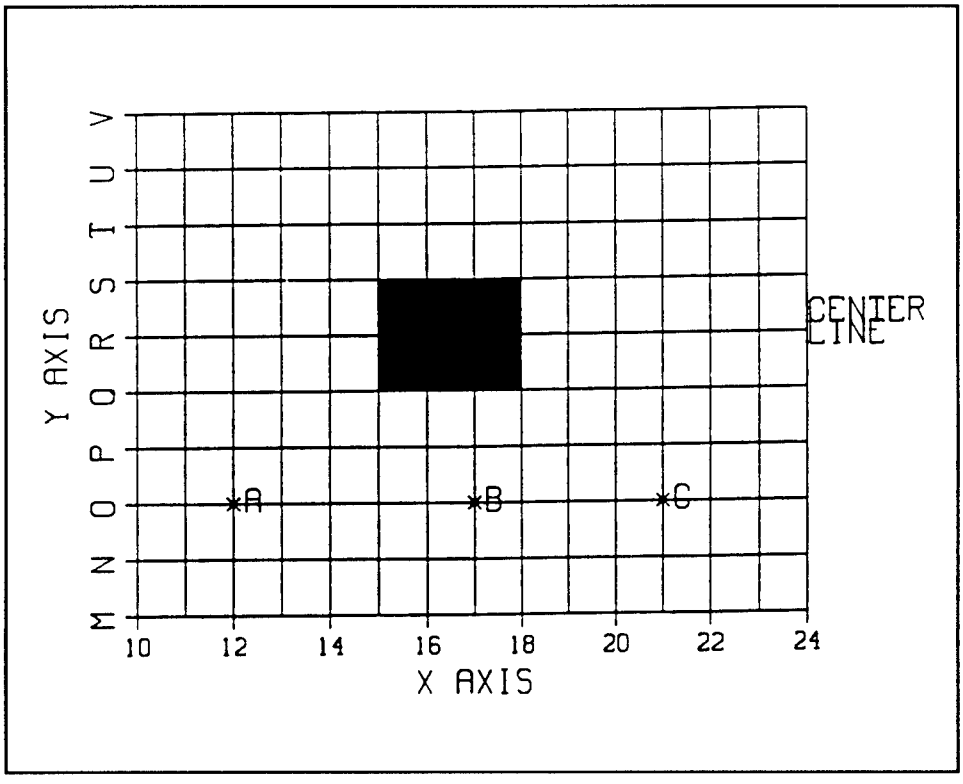

Figure 17. Location of sediment bottles poles for Test No. 1H

Table 15
Comparison of Computed and Measured Suspended Sediment Concentration (mg/ℓ) at Pole B After 15 Seconds

Depth (ft)	Horizontal Position Relative to Point of Discharge (ft)						
	0	1	2	3	4	5	6
1.0	14900	21500	200	0	0	0	0
	21500	5800	35	0	0	0	0
	200	35	0	0	0	0	0
	(529)						
	0	0	0	0	0	0	0
1.5	73000	104000	4700	80	0	0	0
	104000	33000	2000	30	0	0	0
	4700	2000	170	0	0	0	0
	(421)						
	80	30	0	0	0	0	0
Depth (ft)	0	1	2	3	4	5	6
1.75	29100	58400	18100	3300	210	5	0
	58400	37200	13200	4800	710	40	0
	18100	13200	4800	710	40	0	0
	(1806)						
	3300	2300	710	90	5	0	0

Table 16
Comparison of Computed and Measured Suspended Sediment Concentration (mg/ℓ) at Pole A After 27 Seconds

Depth (ft)	Horizontal Position Relative to Point of Discharge (ft)				
	0	1	2	3	4
1.0	1960	540	0	0	0
	540	25	0	0	0
	0	0	0	0	0
			(1271)		

(Continued)

Table 16 (Concluded)

Depth (ft)	Horizontal Position Relative to Point of Discharge (ft)				
	0	1	2	3	4
1.0	0	0	0	0	0
1.5	23400	39800	2900	20	0
	2900	1100	50	0	0
			(971)		
	20	5	0	0	0
1.75	56000	113000	17000	700	0
	113000	61000	9100	350	0
	17000	9100	1300	40	0
			(974)		
	700	350	40	0	0

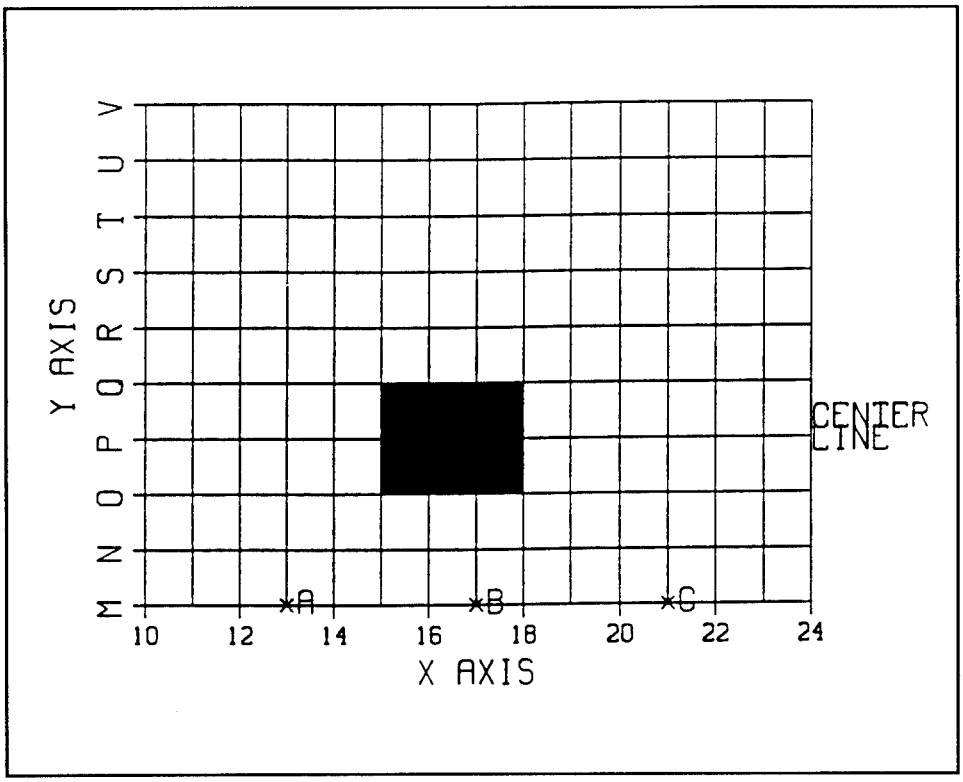

Figure 18. Location of sediment bottles poles for Test No. 5H

Table 17
Comparison of Computed and Measured Suspended Sediment Concentration (mg/ℓ) at Pole C After 11 Seconds

Depth (ft)	Horizontal Position Relative to Point of Discharge (ft)						
	0	1	2	3	4	5	6
1.0	1140	860	0	0	0	0	0
	860	90	0	0	0	0	0
	0	0	0	0	0	0	0
				(737)			
	0	0	0	0	0	0	0
2.0	6500	15300	6500	540	10	0	0
	15300	13000	4200	310	5	0	0
	6500	4200	930	55	0	0	0
				(203)			
	540	310	55	0	0	0	
3.0	10800	25100	12700	3000	370	30	0
	25100	21800	9500	2200	280	20	0
	12700	9500	4000	910	110	10	0
				(738)			
	3000	2200	910	210	30	0	0
3.75	8000	16900	17600	10600	4400	1300	0
	16900	18600	16200	9400	3800	1100	0
	17600	16200	11900	6500	2500	700	0
				(4091)			
	10600	9400	6500	3300	1300	340	0

Tables 15-16, several rows of computed concentrations are presented at each depth. It can be seen that computed and measured results usually agree quite well within one grid point.

The observed bottom deposition covered virtually the entire test section. Model results substantiated this with the maximum computed thickness being 4.2×10^{-3} ft.

Table 18
Comparison of Computed and Measured Suspended Sediment Concentration at Pole B After 20 Seconds

Depth (ft)	Horizontal Position Relative to Point of Discharge (ft)						
	0	1	2	3	4	5	6
1.0	1730	860	0	0	0	0	0
	860	70	0	0	0	0	0
	0	0	0	0	0	0	0
	(89)						
	0	0	0	0	0	0	0
2.0	2700	5870	2520	250	5	0	0
	5870	4820	1680	150	3	0	0
	2520	1680	410	30	0	0	0
	(18)						
	250	150	3	0	0	0	0
	5	3	0	0	0	0	0
3.0	9500	21500	7500	2500	570	70	0
	21500	16000	560	200	45	5	0
	7500	560	300	110	25	3	0
	(15)						
	250	200	110	35	7	0	0
	55	45	25	7	0	0	0
	7	5	3	0	0	0	0
3.75	3190	6100	7190	5700	3800	2420	1390
	6100	6920	7010	5370	3600	2300	1320
	7190	7010	6050	4490	3090	1990	1120
	(2015)						
	5700	5370	4490	3420	2420	1540	850
	3800	3600	3090	2420	1710	1060	570
	2420	2300	1990	1540	1060	640	330
	1390	1320	1120	850	570	330	160

4 Summary and Conclusions

Summary

Numerical models are required to assess water column environmental impacts of dredged material disposals in open water. Such short-term fate models also provide estimates of the initial deposition of sediments that are then used in determining the long-term movement of material within the disposal site. The earliest development of a comprehensive numerical model for predicting the physical fate of material disposed in the ocean was the work of Koh and Chang (1973). However, even though additional developments of the Koh and Chang model continued over the next several years, deficiencies still remained at the initiation of the US Army Corps of Engineers Dredging Research Program (DRP) in 1988.

To provide guidance on removing these deficiencies, large scale (1:50) laboratory tests of split-hull barge and hopper dredge disposals were conducted under the DRP. Results from these tests are presented by Johnson, et al. (1993). The numerical model that has evolved from the DRP is called STFATE (Short-Term FATE). In addition to guiding model developments, results from the laboratory tests have been employed to assess the ability of STFATE to accurately simulate open water disposal operations.

Efforts to remove model deficiencies included developments in the following areas: (a) computation of insertion velocity, (b) dynamic collapse on the bottom, (c) effect of bottom slope, (d) disposal at dispersive sites, (e) consolidation and hopper dredge disposal, (f) stripping of sediment and fluid, (g) time-varying fall velocities, and (h) distribution of bottom deposits. These developments have resulted in a more realistic simulation of real disposal operations. For example, the use of multiple convecting clouds allows for a realistic simulation of disposal from hopper dredges and/or the effect of consolidation of material during transit to the disposal site.

Results from model simulations of seven disposal tests have been presented. These include five disposals from the model split-hull barge and two from the multiple-bin disposal vessel. Water depths ranged from 2.0 to 6.0 ft and sediment types were sand, silt, clay, and fine crushed coal. At a 1 to 50 scale, these tests represented disposal of about 4,000 cu yd from the split-hull barge

and 8,000 cu yd from the hopper dredge type vessel in water depths of 100-300 ft.

Conclusions

From an inspection of the model results compared with measured data from the disposal tests, it can be concluded that STFATE simulates the fate of material disposed in open water well. Average computed and measured descent speeds compared to within 25 percent and average bottom surge speeds compared to within about 10 percent. Considering the idealized geometrical shapes assumed in STFATE and the uncertainty of material characteristics and the manner in which material leaves the disposal vessel, i.e. the initial conditions, these comparisons seem reasonable.

All of the numerical model simulations allowed sediment to be stripped. Computed results for the silt and clay disposals showed about 2-3 percent of the solids being stripped during descent. These results agree with published estimated percentages of stripped material.

When comparing computed and measured suspended sediment concentrations collected by the sediment bottles, it should be realized that small differences in timing and the location of the bottles are extremely important. In addition, the manner in which material leaves the vessel is important. In some tests, small "globs" of material left the vessel after the main body of the descending jet had impacted the bottom. Although the concept of multiple-convecting clouds allows for the effect of consolidation, the behavior described above is impossible to predict.

Suspended sediment results from the disposal of sand in 4.5 ft of water from the model barge compared well with computed results near the bottom. Both computed and measured concentrations were about 17,000 mg/ℓ. However, computed concentrations were too high in the upper water column. Perhaps stripping of sand should not have been allowed.

Computed concentrations of crushed coal disposed in 6.0 ft of water compared well at virtually all locations. Near the point of discharge, measured concentrations varied from about 20 to 18,000 mg/ℓ over the water column. Computed values ranged from near zero to about 17,000 mg/ℓ. At a location farther from the discharge, measured concentrations ranged from 25 to 4,600 mg/ℓ, whereas, computed values ranged from zero near the surface to 3,000 mg/ℓ near the bottom.

Computed and measured concentrations for the clay disposal in 6.0 ft of water compared extremely well throughout the water column away from the point of discharge. These concentrations were in the 50-1,000 mg/ℓ range.

Two simulations of the disposal of a silt mixture from the model barge in water depths of 2.6 and 4.0 ft of water were conducted. Comparisons of

concentrations were excellent close to the discharge point for disposal in 2.6 ft of water with concentrations in the 500-3,500 mg/ℓ range. However, away from the disposal site, model results were too low in the upper water column. Comparisons for the 4.0-ft disposal were opposite from those for the disposal in 2.6 ft of water. Model results showed concentrations ranging from 500-6,000 mg/ℓ near the discharge point with measured data being in the 500-2,000 mg/ℓ range. At a location slightly farther away, both computed and measured concentrations were in the 1,000-2,500 mg/ℓ range. These differences can be attributed to the circular torus shape of the bottom surge and the manner in which STFATE attempts to model it.

Results from the multi-bin disposals showed that computed results generally compared well with measured values near the bottom, but were too low in the upper water column. This was true for disposal in both 2.0 ft and 4.0 ft of water. Again, it appears the shape of the surge is responsible for the differences.

For most of the disposal tests, a comparison of the bottom deposition could only be accomplished in a qualitative sense since the depth of deposition was too small to measure. However, model results generally agreed well in a qualitative sense with observed areas of deposition.

Results from these simulations have substantiated that STFATE can be used to accurately simulate the fate of material during disposal operations. Descent and bottom surge speeds, stripping, rates of dilution, total depositional areas and suspended sediment concentrations in the bottom surge are all reasonably reproduced. However, it is recommended that further attention be given to more accurately represent the effect of the torus shape of the bottom surge.

An example of additional research that is needed to make STFATE even more useful for addressing environmental issues lies in the area of uncertainty. Given the uncertainty in specifying characteristics of the disposal material at the moment of disposal, the manner in which material leaves the disposal vessel, and ambient conditions, an uncertainty analysis should be conducted to better define bounds on the accuracy of predicted water column effects.

5 References

Bokuniewicz, H. J., Gilbert, J., Gordon, R. B., Higgins, J. L., Kaminsky, P., Pilbeam, C. C., Reed, M., and Tuttle, C. (1978). "Field study of the mechanics of the placement of dredged material at open-water disposal sites. Vol. 1: Main text and appendices A-I," Technical Report D-78-7, U.S. Army Engineer Waterways Experiment Station, Vicksburg, MS.

Bowers, G. W., and Goldenblatt, M. K. (1978). "Calibration of a predictive model for instantaneously discharged dredged material," EPA-600/3-78-089, U.S. Environmental Protection Agency, Corvallis, OR.

Brandsma, M. G., and Divoky, D. J. (1976). "Development of models for prediction of short-term fate of dredged material discharged in the estuarine environment," Contract Report D-76-5, U.S. Army Engineer Waterways Experiment Station, Vicksburg, MS; prepared by Tetra Tech, Inc., Pasadena, CA.

Brandsma, M. G., and Sauer, T. C., Jr. (1983). "Mud discharge model: report and user's guide," Exxon Production Research Co., Houston, TX.

Hoerner, S. F. (1965). *Fluid Dynamic Drag*, published by author, Brick Town, New Jersey.

Johnson, B. H. (1990). "User's guide for models of dredged material disposal in open water," Technical Report D-90-5, U.S. Army Engineer Waterways Experiment Station, Vicksburg, MS.

Johnson, B. H., McComas, D. N., McVan, D. C., and Trawle, M. J. (1993). "Development and verification of numerical models for predicting the Initial fate of dredged material disposed in open water. Report 1 - Physical model tests of dredged material disposal from a split-hull barge and a multiple bin vessel," Technical Report DRP-93-1, U.S. Army Engineer Waterways Experiment Station, Vicksburg, MS.

Koh, R. C. Y., and Chang, Y. C. (1973). "Mathematical model for barged ocean disposal of waste," Technical Series EPA 660/2-73-029, U.S. Environment Protection Agency, Washington, DC.

Kraus, N. C. (1991). "Mobile Alabama, field data collection project, 18 August - 2 September 1989 - Report 1 - Dredged material plume survey data report," Technical Report DRP-91-3, U.S. Army Engineer Waterways Experiment Station, Vicksburg, MS.

Madsen, O. S. and Wikramanayake, P. N. (1991). "Simple models for turbulent wave-current bottom boundary layer flow," Contract Report DRP-91-1, U.S. Army Engineer Waterways Experiment Station, Vicksburg, MS.

Moritz, H. R., and Randall, R. E. (1992). "Users guide for the open water disposal area management simulation," Contract Report DACW39-90-K-0015, Texas A&M University, College Station, TX.

Scorer, R. S. (1957). "Experiments on convection of isolated masses of buoyant fluid," *Journal of Fluid Mechanics*, Vol. 2, p. 583.

Turner, J. S. (1960). "A Comparison between buoyant vortex rings and vortex pairs," *Journal Fluid Mechanics*, Vol. 7, pp. 419-432.

Woodward, B. (1959). "Motion in and around isolated thermals," *Quarterly Journal of Royal Meteorological Society*, Vol. 85, p. 144.

REPORT DOCUMENTATION PAGE

Form Approved
OMB No. 0704-0188

1. AGENCY USE ONLY *(Leave blank)*	2. REPORT DATE	3. REPORT TYPE AND DATES COVERED
	February 1995	Final report

4. TITLE AND SUBTITLE
Development and Verification of Numerical Models for Predicting the Initial Fate of Dredged Material Disposed in Open Water; Report 2, Theoretical Developments and Verification Results

5. FUNDING NUMBERS
WU 32465

6. AUTHOR(S)
Billy H. Johnson, Moira T. Fong

7. PERFORMING ORGANIZATION NAME(S) AND ADDRESS(ES)
U.S. Army Engineer Waterways Experiment Station
3909 Halls Ferry Road, Vicksburg, MS 39180-6199

8. PERFORMING ORGANIZATION REPORT NUMBER
Technical Report DRP-93-1

9. SPONSORING/MONITORING AGENCY NAME(S) AND ADDRESS(ES)
U.S. Army Corps of Engineers
Washington, DC 20314-1000

10. SPONSORING/MONITORING AGENCY REPORT NUMBER

11. SUPPLEMENTARY NOTES
Available from National Technical Information Service, 5285 Port Royal Road, Springfield, VA 22161.

12a. DISTRIBUTION/AVAILABILITY STATEMENT
Approved for public release; distribution is unlimited.

12b. DISTRIBUTION CODE

13. ABSTRACT *(Maximum 200 words)*

A numerical model called STFATE for computing the short-term fate of dredged material disposed in open water has been developed. STFATE builds upon work of earlier researchers to provide a more realistic simulation of real disposal operations from split-hull barges and multi-bin hopper dredges. New developments allow for multiple-convecting clouds and stripping of solids fluid from those clouds to better represent water column effects. Other developments include the use of the total energy approach for computing the bottom surge and computations that make the model more applicable at dispersive disposal sites.

STFATE has been applied to simulate disposal tests conducted at a 1:50 scale in a large laboratory facility at the U.S. Army Engineer Waterways Experiment Station. Comparison of computed and measured results on decent and bottom surge speeds, bottom deposition, and suspended sediment concentrations have been made. The results show that STFATE can be used to reliably predict the fate of material disposed at open water disposal sites. However, an uncertainty analysis is needed to place accuracy bounds on model results.

14. SUBJECT TERMS

Barge	Hopper dredge	Sediment
Disposal	Mixing zone	
Dredged material	Numerical model	

15. NUMBER OF PAGES
74

16. PRICE CODE

17. SECURITY CLASSIFICATION OF REPORT	18. SECURITY CLASSIFICATION OF THIS PAGE	19. SECURITY CLASSIFICATION OF ABSTRACT	20. LIMITATION OF ABSTRACT
UNCLASSIFIED	UNCLASSIFIED		